

1 **The deubiquitinase Usp9x regulates PRC2-mediated chromatin reprogramming during**
2 **mouse development**

3
4 Trisha A. Macrae^{1,2,3}, Miguel Ramalho-Santos^{1,2,3,4*}

5
6 **Author information:**

7 ¹Eli and Edythe Broad Center of Regeneration Medicine and Stem Cell Research, University of
8 California, San Francisco, San Francisco, CA, USA.

9 ²Center for Reproductive Sciences, University of California, San Francisco, San Francisco, CA,
10 USA.

11 ³Present address: Lunenfeld-Tanenbaum Research Institute, Mount Sinai Hospital, Toronto,
12 Ontario, Canada.

13 ⁴Department of Molecular Genetics, University of Toronto, Toronto, Ontario, Canada.

14 *email: mrsantos@lunenfeld.ca.

15
16
17 **ABSTRACT**

18
19 Pluripotent cells of the mammalian embryo undergo extensive chromatin rewiring to prepare for
20 lineage commitment after implantation. Repressive H3K27me₃, deposited by Polycomb
21 Repressive Complex 2 (PRC2), is reallocated from large gene-distal blankets in pre-implantation
22 embryos to mark promoters of developmental genes. The factors that mediate this global
23 redistribution of H3K27me₃ are unknown. Here we report a post-translational mechanism that
24 destabilizes PRC2 to constrict H3K27me₃ during lineage commitment. Using an auxin-inducible
25 degron system, we show that the deubiquitinase Usp9x is required for mouse embryonic stem
26 (ES) cell self-renewal. Usp9x-high ES cells have high PRC2 levels and bear a chromatin and
27 transcriptional signature of the pre-implantation embryo, whereas Usp9x-low ES cells resemble
28 the post-implantation, gastrulating epiblast. We show that Usp9x interacts with, deubiquitinates
29 and stabilizes PRC2. Deletion of *Usp9x* in post-implantation embryos results in the derepression
30 of genes that normally gain H3K27me₃ after gastrulation, followed by the appearance of
31 morphological abnormalities at E9.5, pointing to a recurrent link between Usp9x and PRC2 during
32 development. Usp9x is a marker of “stemness” and is mutated in various neurological disorders
33 and cancers. Our results unveil a Usp9x-PRC2 regulatory axis that is critical at peri-implantation
34 and may be redeployed in other stem cell fate transitions and disease states.

35 INTRODUCTION

36

37 Immediately after implantation, the pluripotent embryonic epiblast enters a period of accelerated
38 growth. This amplification event corresponds to a transition in cell fate from a pre-implantation
39 state of naïve pluripotency to a post-implantation state of lineage priming. The stages of
40 pluripotency can be modeled in vitro using mouse Embryonic Stem (ES) cells: culture in dual
41 Mek/Gsk3 β inhibition with leukemia inhibitory factor (LIF) and vitamin C maintains a pre-
42 implantation-like state of pluripotency¹⁻³, while ES cells in serum/LIF mimic the fast-growing state
43 of early post-implantation epiblast cells^{4,5}.

44

45 Reprogramming of the chromatin landscape contributes to the transition in pluripotent cell states
46 at peri-implantation⁶. This reprogramming event includes a global redistribution of the repressive
47 histone mark H3K27me3, deposited by Polycomb Repressive Complex 2 (PRC2). Recent studies
48 document that H3K27me3 marks broad genic and intergenic domains in pre-implantation
49 embryos as well as naïve ES cells⁷⁻⁹. After implantation, H3K27me3 becomes concentrated over
50 promoters of developmental regulatory genes^{7,10}, resembling patterns that restrain expression of
51 bivalent (H3K27me3/H3K4me3-marked) genes in serum ES cells^{11,12}. The mechanisms that
52 regulate this peri-implantation switch in PRC2 activity are unknown.

53

54 We recently reported a genome-wide screen that revealed that the chromatin state of ES cells is
55 acutely tuned to variations in protein synthesis and degradation⁵. The deubiquitinating enzyme
56 Ubiquitin Specific Protease 9x (Usp9x) was one of the top hits in this screen. Although its roles in
57 chromatin regulation have not been investigated, Usp9x is a marker of “stemness”^{13,14} and is a
58 key, conserved regulator of several stem/progenitor cells, including neural¹⁵⁻¹⁸, hematopoietic¹⁹,
59 muscle²⁰ and intestinal cells²¹. For example, Usp9x promotes self-renewal of mouse neural
60 stem/progenitor cells^{15,18}, and *USP9X* mutations are implicated in X-linked neurodevelopmental
61 syndromes²²⁻²⁴, Turner Syndrome²⁵, intellectual disability²⁶ and seizures²⁷ (reviewed in ref. 28).
62 Moreover, *USP9X* mutations occur frequently in human cancers²⁹⁻³¹. We report here that Usp9x
63 deubiquitinates and stabilizes PRC2, acting as a gatekeeper to the switch in H3K27me3
64 deposition patterns during mouse development. These findings shed light on the regulation of
65 chromatin reprogramming in pluripotent cells and during lineage commitment, and have important
66 implications for physiological and pathological settings where Usp9x and PRC2 have been shown
67 to play roles.

68 RESULTS

69

70 **Usp9x promotes ES cell self-renewal and a transcriptional state of pre-implantation**

71 We established an auxin inducible degron (AID) system for acute control of Usp9x protein
72 levels^{32,33} (Fig. 1a). In ES cells homozygous for the *OsTir1* auxin receptor, we tagged
73 endogenous *Usp9x* with enhanced green fluorescent protein (GFP) and a minimal AID or 3x Flag
74 tag (herein referred to as AID-Usp9x or Flag-Usp9x, respectively). Auxin drives substantial Usp9x
75 protein depletion in AID-Usp9x cells within approximately 8 hours (h) (Supplementary Fig. 1a).
76 We used GFP expression to isolate subpopulations that resist degradation (Usp9x-high) or lose
77 Usp9x (Usp9x-low) in response to auxin (Fig. 1a), each fraction corresponding to ~20% of the
78 total population.

79

80 Usp9x-high and Usp9x-low ES cells express comparable levels of Oct4, but Usp9x-low ES cells
81 are Nanog-low and display a 5-fold reduction in self-renewal capacity (Fig. 1b). Knockdown of
82 Usp9x by an alternative method (RNA interference) also induces loss of self-renewal
83 (Supplementary Fig. 1b). Furthermore, Usp9x expression declines with early lineage commitment
84 by Embryoid Body (EB) formation, and low Usp9x expression does not represent a distinct cell
85 cycle stage (Supplementary Fig. 1c-e).

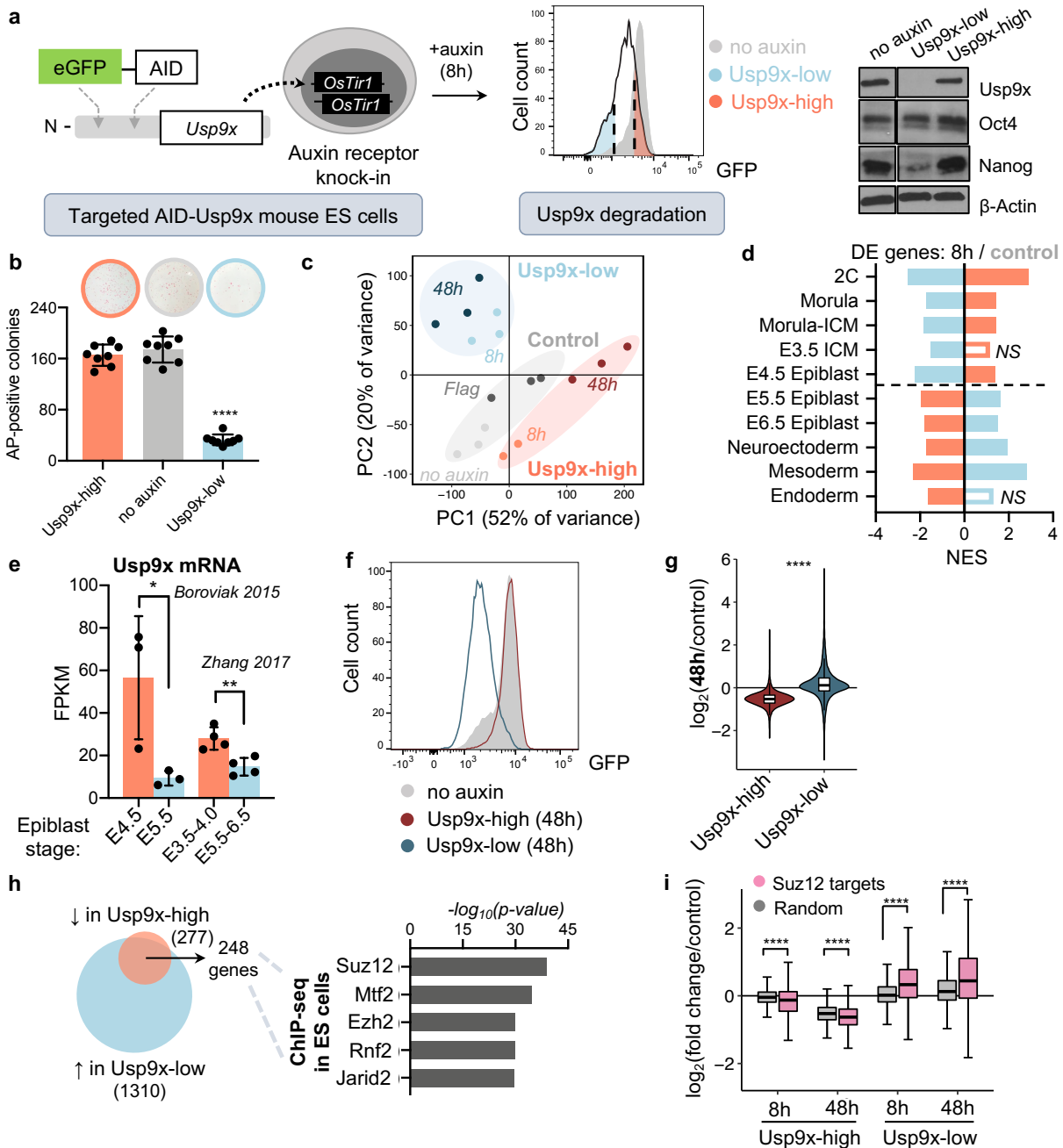
86

87 We performed cell number-normalized (CNN) RNA-sequencing (RNA-seq) with spike-ins to
88 characterize Usp9x-high and Usp9x-low ES cells. By principal component analysis (PCA),
89 replicates cluster according to Usp9x levels (Fig. 1c). We calculated differential expression in 8h
90 Usp9x-high or Usp9x-low ES cells versus controls and compared their profiles to molecular
91 signatures of development using Gene Set Enrichment Analysis (GSEA)³⁴ (Supplementary Table
92 1). This analysis revealed a striking polarity based on Usp9x levels: the Usp9x-high state
93 correlates with pre-implantation embryonic stages, whereas Usp9x-low ES cells resemble the
94 post-implantation epiblast and early lineages (Fig. 1d). Usp9x-high ES cells express high levels
95 of naïve state markers and low levels of primed state markers^{5,35}, while the opposite is observed
96 in Usp9x-low ES cells (Supplementary Fig. 1f,g). Moreover, the expression of Usp9x itself
97 declines from pre- to post-implantation in wild-type embryos (Fig. 1e, Supplementary Fig. 1h)^{36,37}.
98 These results indicate that Usp9x promotes ES cell self-renewal and that loss of Usp9x captures
99 the transcriptional reprogramming that occurs in pluripotent cells at implantation.

100

101 ES cells cultured in serum/LIF represent a heterogeneous mixture of interconvertible pluripotent
102 states. Surprisingly, isolated Usp9x-low cells do not re-distribute along a spectrum of Usp9x
103 expression after a 48h recovery period without auxin (Fig. 1f and Supplementary Fig. 2a), unlike
104 the cases of naïve pluripotency markers such as Nanog or Rex1^{38,39}. Usp9x-high cells settle into
105 a state of *hypotranscription*⁴, demonstrating a suppression of the majority of the transcriptome
106 relative to control cells. By contrast, Usp9x-low cells at 48h show relative *hypertranscription* as
107 well as induction of differentiation- and development-related Gene Ontology (GO) terms (Fig. 1g
108 and Supplementary Fig. 2b,c), similar to the predicted upregulation of transcriptional output and
109 lineage induction in the post-implantation epiblast^{5,40,41}.

110
111 We probed the Usp9x-associated transcriptional signatures for clues to the regulatory networks
112 establishing such divergent cell fates. Consistent with their anti-correlated GSEA signatures (Fig.
113 1d), Usp9x-high and Usp9x-low ES cells show polarized expression of many of the same genes.
114 Of the 277 genes significantly downregulated in Usp9x-high cells, 248 (90%) are significantly
115 upregulated in Usp9x-low cells. ChIP-X Enrichment Analysis (ChEA) revealed that these genes
116 are enriched for targets of Polycomb Repressive Complex 2 (PRC2) (Fig. 1h and Supplementary
117 Fig. 2d)^{42,43}. Deletion of core members (Suz12, Ezh2, or Eed) in ES cells leads to induction of
118 developmental regulatory genes^{44,45} and can promote premature lineage commitment^{46–48},
119 similar to the behavior of Usp9x-low ES cells (Supplementary Fig. 1f). These data indicate that
120 Usp9x-high ES cells represent a PRC2-repressed, pre-implantation state of pluripotency, while
121 activation of a subset of PRC2 targets in Usp9x-low ES cells promotes a post-implantation state
122 of lineage induction (Fig. 1i).



123
 124
 125
 126
 127
 128
 129
 130
 131
 132
 133

Figure 1. Usp9x promotes ES cell self-renewal and a transcriptional signature of pre-implantation linked to PRC2 activity. **a**) Schematic of an auxin-inducible degron (AID) system for acute Usp9x depletion in mouse embryonic stem (ES) cells. Right: western blot confirming endogenous Usp9x depletion in Usp9x-low and retention in Usp9x-high ES cells. **b**) Usp9x-low ES cells show a self-renewal deficit. Representative images and quantification of colony formation assays. AP, Alkaline Phosphatase. **c**) Principal Component Analysis (PCA) of gene expression by RNA-seq. 8h: 8h auxin. No auxin: AID-Usp9x cells with vehicle treatment. 48h: 8h auxin followed by 48h recovery without auxin. Flag: Flag-Usp9x cells after 8h auxin and 48h recovery. **d**) The transcriptional signatures of Usp9x-high or Usp9x-low ES cells correlate with different

134 stages of peri-implantation development by Gene Set Enrichment Analysis (GSEA). See Methods
135 for references. *NES*, Normalized Enrichment Score, *DE*, differentially expressed; *NS*, not
136 significant (FDR > 0.05). **e)** *Usp9x* mRNA expression in the epiblast declines from pre- to post-
137 implantation^{36,37}. **f)** *Usp9x*-low ES cells do not recover *Usp9x* expression after 48h without auxin.
138 **g)** Violin plots of the fold-change in expression of all genes at 48h relative to control cells, showing
139 hypotranscription in *Usp9x*-high ES cells and hypertranscription in *Usp9x*-low ES cells. **h)** The
140 overlap of genes *DE* in *Usp9x*-high and *Usp9x*-low ES cells are enriched for PRC2 binding by
141 Enrichr analysis⁴². **i)** Boxplots showing repression (in *Usp9x*-high) or induction (in *Usp9x*-low) of
142 *Suz12* target genes⁴⁹, compared to a random subset ($n = 3350$).
143 Data are mean \pm s.d. of 4 replicates from 2 sorts (b), mean \pm s.d. (e), mean \pm s.e.m. (i). Boxplot
144 hinges (h, i) show the first and third quartiles, with median center line. * $P < 0.05$, ** $P < 0.01$, **** P
145 $< 2.2 \times 10^{-16}$. P -values by one-way ANOVA with multiple t-test comparisons to the no-auxin
146 condition (b), Student's t-test with Welch's correction (e), Wilcoxon rank-sum test (g), and ANOVA
147 with multiple pairwise Wilcoxon tests (i).

148

149

150

151 ***Usp9x*-mutant embryos arrest at mid-gestation with incomplete repression of a subset of** 152 **PRC2-targeted lineage genes**

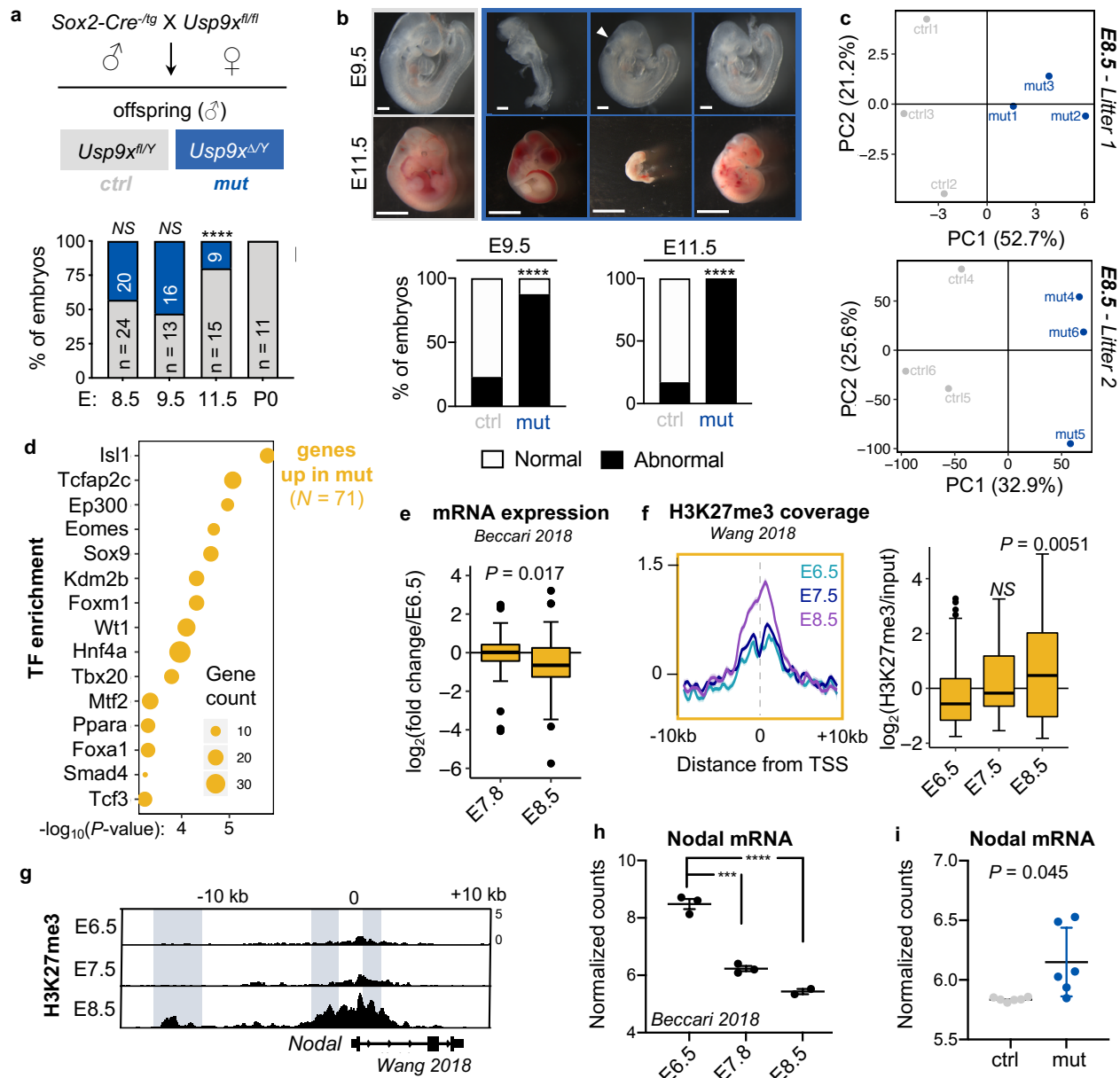
153 We next turned to a mouse model to study the role of *Usp9x* in developmental progression.
154 *Usp9x*-mutant embryos arrest at mid-gestation^{50,51}, although the stage and underlying causes of
155 developmental arrest are unknown. To avoid confounding effects from roles of *Usp9x* in cleavage-
156 stage and trophectoderm development^{52,53}, we used a *Sox2-Cre* to delete *Usp9x* strictly in the
157 post-implantation epiblast derivatives of embryos⁵⁴. We then genotyped and catalogued the
158 morphology of control (ctrl, *Usp9x*^{fl/Y}) versus mutant (mut, *Usp9x* ^{Δ Y}) embryos at several mid-
159 gestation stages (Fig. 2a, Supplementary Fig. 3a). Deviation from the expected (1:1) ratio arises
160 by E11.5, at which point mutants account for only ~25% of recovered embryos and have
161 morphological abnormalities with 100% penetrance. The few mutants that survive to E11.5 show
162 extensive hemorrhaging, while most display pericardial edema, cerebral edema and severe delay,
163 pointing to an earlier developmental arrest (Fig. 2b). *Usp9x* mutants already display
164 developmental delay (delayed turning, open anterior neural tube) or gross abnormalities by E9.5,
165 including blunted posterior trunk development and exencephaly (Fig. 2b). These pleiotropic
166 outcomes agree with the phenotypes of E9.5 chimeric embryos derived from *Usp9x*-genetrapped
167 ES cells and the ubiquitous expression of *Usp9x* at E9.5^{51,55}.

168

169 *Usp9x* mutants appear morphologically normal at E8.5 (Supplementary Fig. 3b). We therefore
170 performed whole-embryo RNA-seq at this stage to identify early transcriptional changes that may

171 anticipate subsequent developmental defects. As expected, the transcriptional differences are
172 relatively minor at this stage: we identified 71 upregulated and 66 downregulated genes in *Usp9x*
173 mutants (Supplementary Fig. 3c,d and Supplementary Table 2). Nevertheless, E8.5 *Usp9x*
174 mutants are readily distinguished from controls by PCA and unsupervised hierarchical clustering
175 (Fig. 2c, Supplementary Fig. 3e). Upregulated genes in *Usp9x* mutants are also upregulated in
176 48h *Usp9x*-low ES cells (Supplementary Fig. 3f). These genes include targets of master
177 developmental transcription factors (*Isl1*, *Tfap2c*, *Eomes*, *Sox9*, *Hnf4a*, among others, Fig. 2d),
178 and are enriched for processes in cardiac/mesoderm and endoderm development
179 (Supplementary Fig. 3g). Overall, the genes upregulated in *Usp9x*-mutants at E8.5 typically
180 decline by this point during wild-type development⁵⁶ (Fig. 2e), suggesting that *Usp9x* is required
181 for appropriate silencing of developmental regulatory genes.

182
183 Incomplete repression of regulators of lineage commitment with defective differentiation is also
184 observed in PRC2-hypomorphic ES cells^{49,57}. Recent chromatin immunoprecipitation-sequencing
185 (ChIP-seq) of wild-type mouse embryos documented a wave of H3K27me3 deposition during
186 gastrulation⁵⁸. We therefore probed the developmental dynamics of H3K27me3 levels at genes
187 differentially expressed in *Usp9x* mutants. Interestingly, the genes upregulated in E8.5 *Usp9x*
188 mutants normally gain significant amounts of H3K27me3 between E6.5 and E8.5 (Fig. 2f),
189 suggesting that PRC2 activity contributes to repressing them (Fig. 2e) at this stage. The TGF β
190 superfamily member *Nodal* is one key gene that normally accumulates H3K27me3 concurrent
191 with its downregulation by E8.5 (Fig. 2g,h). *Nodal* remains upregulated in E8.5 *Usp9x* mutants
192 (Fig. 2i). We speculate that persistent expression of earlier developmental regulators such as
193 *Nodal* may impede developmental progression of *Usp9x* mutant embryos. Consistent with this
194 notion, the 66 genes *downregulated* in mutants are normally induced from E7.5-E8.5
195 (Supplementary Fig. 3h-j). Taken together, these results indicate that E8.5 *Usp9x* mutant embryos
196 display incomplete repression of early post-gastrulation lineage commitment genes that normally
197 gain H3K27me3 at this stage.



198
199
200
201
202
203
204
205
206
207
208
209

Figure 2. *Usp9x*-mutant embryos arrest at E9.5-E11.5 and display defective repression of early lineage programs marked by H3K27me3. **a)** Genetic cross to delete *Usp9x* in epiblast derivatives of post-implantation embryos. Below, quantification of male (XY) embryos at several post-implantation stages. **b)** Representative images and quantification of control and mutant embryo phenotypes. Scale bars = 250 μm (E9.5), 2.8 mm (E11.5). **c)** PCA plots of RNA-seq from litter-matched mutants and controls, showing that genotypes separate along PC1. **d)** Enrichment analysis of the top-enriched transcription factors (TF) that bind to the genes upregulated in *Usp9x*-mutant embryos in various cell types. **e)** Expression of the genes upregulated in *Usp9x* mutants during wild-type development⁵⁶. **f)** Distribution and boxplot quantification of H3K27me3 levels over the genes upregulated in *Usp9x* mutants⁵⁸. **g)** Representative genome browser tracks of H3K27me3 in wild-type embryos (E6.5-E8.5) at the *Nodal* locus⁵⁸. Known enhancer elements are

210 highlighted and show gains of H3K27me3. **h)** Nodal mRNA expression in wild-type
211 development⁵⁶. **i)** Nodal derepression in *Usp9x*-mutant versus control embryos at E8.5.
212 Boxplot hinges (e, f) show the first and third quartiles, with median center line. Data are mean \pm
213 s.e.m. (h, i). *** $P < 0.001$, **** $P < 0.0001$ or indicated. P -values obtained by χ^2 test (a, b), Student's
214 t-test with Welch's correction (e, i), Wilcoxon rank-sum test (f), and ANOVA with multiple t-test
215 comparison to E6.5 (h).

216

217

218

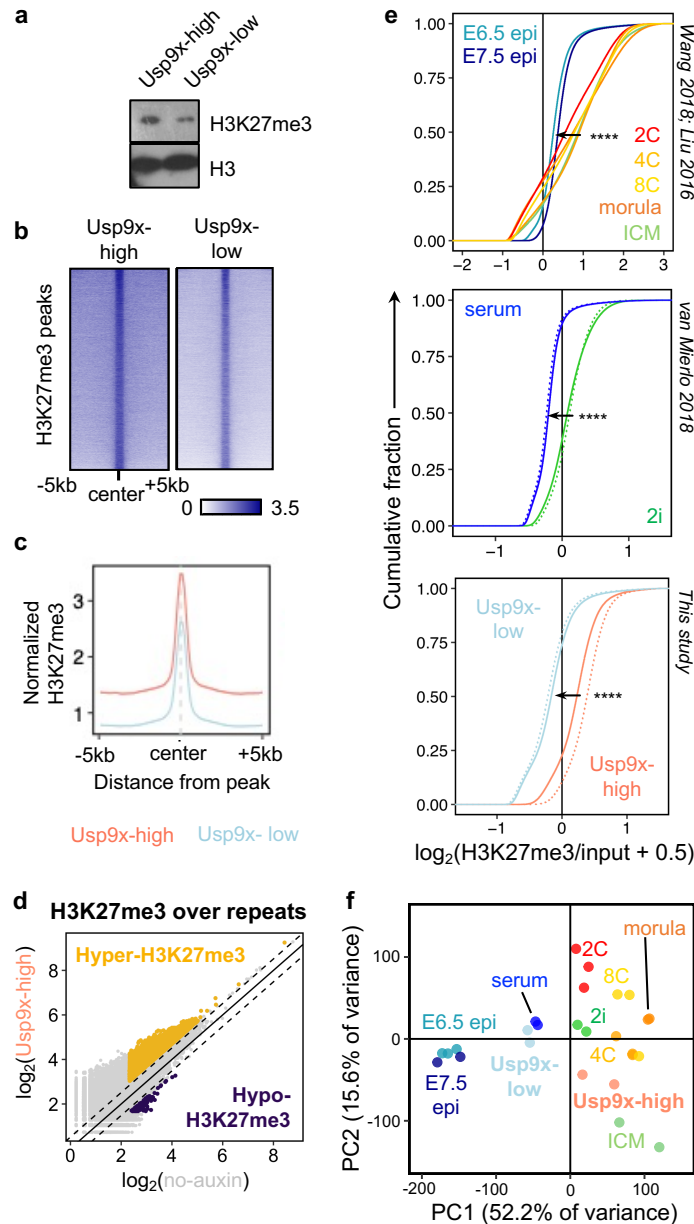
219 **Usp9x mediates a pre- to post-implantation switch in H3K27me3 distribution**

220 Our transcriptional analyses point to a role for *Usp9x* in promoting PRC2-mediated silencing of
221 developmental regulatory genes, both in ES cells to prevent their premature activation prior to
222 lineage commitment (Fig. 1) and in post-gastrulation embryos to allow for subsequent
223 development (Fig. 2). We returned to ES cells to dissect the mechanism by which *Usp9x* regulates
224 PRC2 activity. Consistent with their signature of PRC2 target gene derepression (Fig. 1i), *Usp9x*-
225 low ES cells display globally reduced levels of H3K27me3 compared to *Usp9x*-high ES cells by
226 cell number-normalized western blot (Fig. 3a). We next used spike-in normalized ChIP-seq to
227 map the genome-wide levels and distribution of H3K27me3 between *Usp9x*-associated cell
228 states. Compared to *Usp9x*-low ES cells, *Usp9x*-high ES cells display global gains of H3K27me3
229 at bivalent (dual H3K4me3/H3K27me3-marked) promoters⁵⁹ (Supplementary Fig. 4a-c), which
230 are canonical PRC2 targets highly enriched for developmental regulators. H3K27me3 gains are
231 not limited to bivalent promoters, as *Usp9x*-high cells carry higher levels over peaks present at
232 baseline (no-auxin condition) and spreading upstream and downstream of peaks (Fig. 3b,c and
233 Supplementary Fig. 4d). *Usp9x*-high cells also have H3K27me3 enrichment over repetitive
234 elements (Fig. 3d), which are targeted by this mark in naïve, pre-implantation-like conditions⁶⁰.
235 Thus, the transition from *Usp9x*-high to *Usp9x*-low ES cells involves a genome-wide reduction in
236 H3K27me3 and a narrowing of its peaks across developmental genes and repeat elements.

237

238 The pattern of H3K27me3 in *Usp9x*-high serum ES cells resembles the diffuse domains of the
239 mark in naïve ES cells under dual Mek/Gsk3 β inhibition (2i) and in pre-implantation embryos⁷⁻
240 ^{9,61}. In agreement with this notion, cumulative enrichment plots revealed that the global drop in
241 H3K27me3 levels in *Usp9x*-high versus *Usp9x*-low ES cells recapitulates what is observed in the
242 transition from 2i to serum ES cells and from pre-implantation to post-implantation embryos (Fig.
243 3e). PCA of H3K27me3 ChIP-seq data separates pre-implantation and post-implantation embryos
244 along PC1. ES cell data also follow this trajectory, with *Usp9x*-high and 2i ES cells aligning with

245 pre-implantation and Usp9x-low and serum ES cells clustering with post-implantation stages (Fig.
 246 3f). These results indicate that H3K27me3 enrichment across large swaths of the genome (Fig.
 247 3), together with a PRC2-repressed transcriptional program (Fig. 1), are hallmarks of pre-
 248 implantation pluripotency^{62–64} and Usp9x-high ES cells.
 249



250
 251 **Figure 3. Usp9x mediates a pre- to post-implantation switch in H3K27me3 distribution. a)**
 252 CNN western blot of H3K27me3 from histone extracts, representative of 2 biological replicates.
 253 **b)** Heatmaps of H3K27me3 ChIP-seq signal in Usp9x-high and Usp9x-low ES cells, showing
 254 H3K27me3 spreading in Usp9x-high cells. **c)** Profile plot depicting the mean signal of coverage
 255 shown in (b). **d)** Usp9x-high ES cells carry more H3K27me3 over repetitive elements compared
 256 to untreated (no-auxin) cells. Each point represents an individual element. **e)** Cumulative

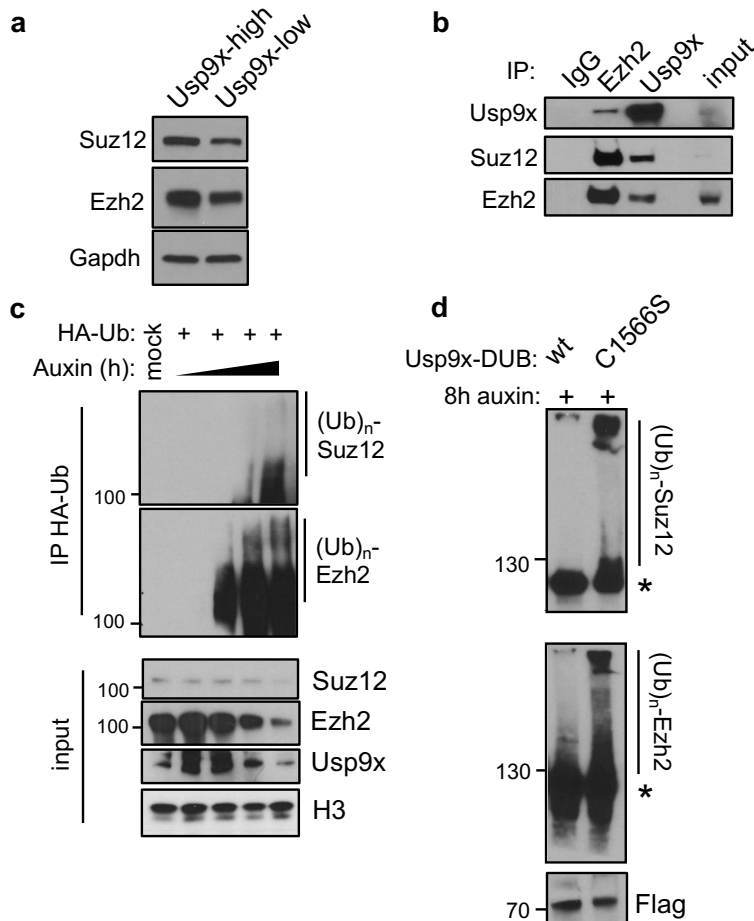
257 enrichment plots of H3K27me3 enrichment in non-overlapping genomic bins of *in vivo*
258 developmental stages (top) and ES cell states (middle, bottom)^{8,58,65}. Pre-implantation stages
259 (2C-ICM, top) or pre-implantation-like ES cell states (2i, Usp9x-high) display H3K27me3
260 enrichment. *Epi*, epiblast. **f**) PCA plots clustering Usp9x-high and Usp9x-low ES cells among the
261 samples shown in (e) based on H3K27me3 distributions. Each point represents a biological
262 replicate. **** $P < 2.2 \times 10^{-16}$ by Kolmogorov-Smirnov test.
263

264

265

266 **Usp9x deubiquitinates and stabilizes PRC2**

267 We next explored the possibility that Usp9x may directly regulate PRC2 levels or activity. We
268 found that the protein levels of core PRC2 components are downregulated in Usp9x-low ES cells
269 (Fig. 4a). This finding led us to hypothesize that Usp9x deubiquitinates and stabilizes PRC2
270 components to drive H3K27me3 deposition. In support of this notion, endogenous Usp9x interacts
271 with Suz12 and Ezh2 in ES cell nuclear extracts (Fig. 4b, Supplementary Fig. 5a). Moreover,
272 acute AID-Usp9x depletion leads to the accumulation of poly-ubiquitinated forms of Suz12 and
273 Ezh2, within 4-8h of auxin addition (Fig. 4c). Alternative methods of reducing Usp9x activity, either
274 small molecule inhibition (WP1130)⁶⁶ or overexpression of a mutant catalytic domain (C1566S),
275 also lead to accumulation of ubiquitinated forms of Suz12 and Ezh2 (Fig. 4d and Supplementary
276 Fig. 5b,c). These gains of ubiquitin upon Usp9x loss correlate with destabilization of Suz12 and/or
277 Ezh2 (Fig. 4a,c-d and Supplementary Fig. 5b,c). Taken together, these data indicate that Usp9x
278 interacts with PRC2 components and that its catalytic activity is required to promote a
279 deubiquitinated state and higher protein levels of PRC2.



280
281
282
283
284
285
286
287
288
289
290
291

Figure 4. Usp9x is a PRC2 deubiquitinase. a) CNN western blots for Suz12 and Ezh2 proteins in whole cell extracts. **b)** Co-immunoprecipitation (IP) and western blot showing a reciprocal interaction between endogenous Ezh2 and Usp9x in wild-type ES cells. **c)** Acute auxin depletion over a time course from 0-8h leads to gain of ubiquitinated species of Suz12 and Ezh2 and destabilization of their protein levels. *HA-Ub*, HA-tagged ubiquitin; $(Ub)_n$, polyubiquitination. **d)** Overexpressing a catalytic-mutant (C1566S) versus wild-type (wt) form of the Usp9x catalytic domain (DUB) leads to gain of Suz12 and Ezh2 ubiquitin levels. AID-Usp9x cells were treated with auxin for 8h to deplete endogenous Usp9x. Asterisk (*) designates the expected sizes for non-ubiquitinated species. Western blots are representative of at least 2 biological replicates.

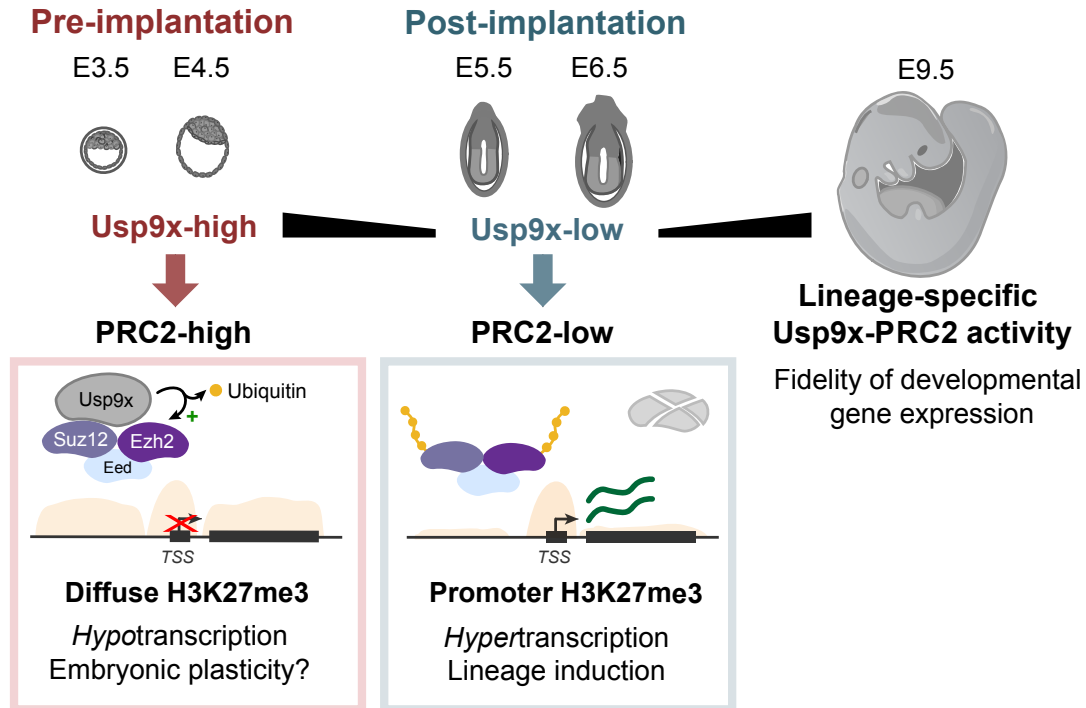
292 **DISCUSSION**

293

294 In summary, we report here that Usp9x deubiquitinates core PRC2 members to promote high
295 levels of H3K27me3, repress developmental regulatory genes and maintain a pre-implantation-
296 like state in ES cells (Fig. 5). Studies in mammalian systems have emphasized the developmental
297 role of PRC2 in regulating bivalent promoters^{11,12}, which represent the highest-affinity sites for
298 PRC2 activity^{61,67,68}. However, H3K27me3 is widespread outside of bivalent chromatin over the
299 genomes of pre-implantation embryos and Usp9x-high ES cells, and broad domains occur in other
300 cell types later in development⁶⁹⁻⁷². Promiscuous activity may be an ancestral function of PRC2⁷³.
301 While the mechanisms underlying such promiscuity remain unclear, the Eed subunit has been
302 shown to promote spreading of H3K27me3 domains⁷⁴. PRC2 stability may also be a major
303 factor⁷⁵. Oncogenic *EZH2* mutations stabilize the complex and cause ectopic gains of H3K27me3
304 in lymphoma⁷⁶⁻⁷⁸. Our results highlight a mechanism whereby Usp9x- stabilizes the PRC2
305 complex to promote global increases in H3K27me3 and expansion to lower-affinity sites (Fig. 5).
306 It will be of interest to determine how the partnership between Usp9x and PRC2 integrates with
307 the activity of other Usp9x substrates, as well as to identify the E3 ubiquitin ligase(s) acting on
308 PRC2 during development.

309

310 Maternally-inherited H3K27me3 domains have been proposed to mediate non-canonical genomic
311 imprinting in mouse embryos^{79,80} and restrict enhancer expression in early-stage fly embryos⁸¹.
312 Our finding that Usp9x-high/PRC2-high ES cells enter a state of global hypotranscription (Fig. 1f,i
313 and Supplementary Fig. 2b) raises the possibility that ubiquitous H3K27me3 *in vivo* suppresses
314 large-scale transcription prior to implantation (Fig. 5), possibly by preventing H3K27
315 acetylation^{43,82,83}. Extensive H3K27me3 may also safeguard embryonic potential during
316 segregation of extraembryonic lineages⁶².



317
 318 **Figure 5. Model for the Usp9x-PRC2 regulatory axis in early development.** Usp9x is a PRC2
 319 deubiquitinase that promotes diffuse H3K27me3 deposition and a pre-implantation-like
 320 transcriptional state. Loss of Usp9x leads to PRC2 destabilization, restricted H3K27me3
 321 deposition and global hypertranscription with priming of post-implantation lineages. After
 322 gastrulation, *Usp9x* is required for timely silencing of developmental genes that are PRC2 targets
 323 and for normal development beyond E8.5.

324
 325
 326 Our data suggest that the decline in Usp9x expression at implantation contributes to destabilizing
 327 PRC2 to allow lineage induction. The roles of PRC2 after gastrulation remain obscure. In
 328 zebrafish and *Xenopus*, H3K27me3 marks spatially-regulated genes after gastrulation^{84,85}.
 329 Constitutive *PRC2* knockouts in mouse are peri-gastrulation lethal^{86–88}, but these findings are
 330 confounded by requirements for PRC2 in extraembryonic tissues⁸⁹, and the developmental
 331 consequences of epiblast-targeted PRC2 knockouts are unknown. Intriguingly, recent studies
 332 indicate that re-establishment of H3K27me3 after gastrulation may also regulate spatial gene
 333 expression in mouse^{90,91}. Together with the data presented here, these results suggest that
 334 Usp9x and PRC2 are re-deployed to promote timely H3K27me3 deposition and silencing of key
 335 developmental genes after lineage commitment (Fig. 5). Further studies are required to
 336 understand how Usp9x may regulate batteries of PRC2 target genes in a lineage-specific manner
 337 during organogenesis.

338 The transition from a pre-implantation to a post-implantation state of pluripotency mirrors stem
339 cell expansion events in other compartments. Supporting the designation of Usp9x as a
340 “stemness” factor^{13,14}, loss-of-function studies document that Usp9x restricts premature
341 expansion of embryonic (this study), neural^{17,18}, hematopoietic¹⁹ and intestinal stem/progenitor
342 cell compartments²¹ in mice. Similarly, PRC2 plays essential roles in each of these stem cell
343 compartments^{92–95}. Mutations in *USP9X* are associated with several neurodevelopmental and
344 neurodegenerative disorders as well as cancers^{22,23,26–31,96}. Thus, the Usp9x-PRC2 axis
345 reported here merits further exploration in other developmental contexts and disease states.

346 **ACKNOWLEDGMENTS**

347 We thank Aydan Bulut-Karslioglu and members of the Santos laboratory for input and critical
348 reading of the manuscript. We are grateful to Elphège Nora and Benoit Bruneau for the AID
349 targeting vector and *OsTir1*-knockin ES cells. We also thank J. Lee and the Toronto Center for
350 Phenogenomics for mouse colony maintenance and support; M. Abed and V. Dixit for sharing the
351 *Usp9x*-flox mice; E. Chow, K. Chan, and members of the UCSF Center for Advanced Technology
352 and the LTRI Sequencing Core for next-generation sequencing; D. Gökbuget for sonication
353 assistance; S. Biechele for cloning advice; and M. Percharde for bioinformatics guidance. Flow
354 cytometry and sorting were performed in the UCSF Parnassus Flow Cytometry Core, supported
355 by a Diabetes Research Center Grant and National Institutes of Health (NIH) grant P30
356 DK063720. This work was supported by NIH grant 1F30HD093116 (to T.A.M.) and NIH grants
357 R01GM113014 and R01GM123556, a Canada 150 Research Chair in Developmental
358 Epigenetics, and the Medicine by Design Program of the University of Toronto (to M.R.-S).

359

360 **AUTHOR CONTRIBUTIONS**

361 T.A.M. and M.R.-S. conceived of the project. T.A.M. designed, performed, and analyzed all
362 experiments. M.R.-S. supervised the project. T.A.M. and M.R.-S. wrote the manuscript.

363

364 **COMPETING INTERESTS**

365 The authors declare no competing interests.

366

367 **CODE AVAILABILITY**

368 Custom R codes used for data analysis are available upon request.

369

370 **DATA AVAILABILITY**

371 RNA-seq and ChIP-seq data have been deposited in Gene Expression Omnibus (GEO).

372 **METHODS**

373

374 **Mice**

375 *Usp9x^{fl/fl}* females were maintained as homozygotes on a C57BL/6 background by crossing
376 *Usp9x^{fl/fl}* and *Usp9x^{fl/Y}* mice¹⁹. Heterozygous male *Sox2-Cre* mice were obtained from Jackson
377 Laboratories (JAX stock #008454) and bred with Cre-negative females to maintain a stock of
378 heterozygous males⁵⁴. All mice were maintained on 12h light/dark cycle and provided with food
379 and water *ad libitum* in individually ventilated units (Techniplast) in specific pathogen-free facilities
380 at The Center for Phenogenomics, Toronto. All procedures involving animals were performed
381 according to the Animals for Research Act of Ontario and the Guidelines of the Canadian Council
382 on Animal Care. Animal Care Committee reviewed and approved all procedures conducted on
383 animals at TCP (Protocol 22-0331). Sample size choice was not pre-determined.

384

385 Yolk sacs were dissected from embryos and used for DNA extraction with the Red Extract-N-Amp
386 kit (Sigma). *Usp9x* status was assessed by PCR using Phire Green Hot Start II PCR Master Mix
387 (Thermo Fisher Scientific). Cycling conditions: 98°C for 30 sec; 35 cycles of 98°C for 5 sec, 58°C
388 for 5 sec, 72°C for 8 sec; 72°C for 1 min. See Supplementary Table 3 for primer sequences.

389

390 **Plasmid construction**

391 An sgRNA was designed to target the *Usp9x* ATG with 20 nucleotide overhang in both directions.
392 Cloning was performed by annealing pairs of oligos into pSpCas9(BB)-2A-GFP (PX458) (modified
393 from GFP to BFP by site directed mutagenesis), a gift from Feng Zhang (Addgene plasmid #
394 48138; <http://n2t.net/addgene:48138>; RRID:Addgene_48138)⁹⁷. Plasmid identity was verified by
395 Sanger sequencing.

396

397 The eGFP-AID-*Usp9x* plasmid was assembled from a pEN458-eGFP-AID[71-114]-eGFP-CTCF
398 N-terminal targeting construct (a gift from the B. Bruneau lab). The N-terminus was chosen for
399 targeting due to repetitive sequences at the *Usp9x* C-terminus. The vector was digested with NruI,
400 NsiI and XhoI and gel purified to remove regions of *CTCF* homology (Qiagen Gel Extraction kit).
401 ~900 bp homology arms to *Usp9x* were amplified from mouse genomic DNA using PrimeStar
402 GXL polymerase (Takara, CA, USA) and Gibson assembly primers with 21 nucleotide overlap to
403 adjacent fragments. The vector fragments and homology arms were cloned by Gibson Assembly
404 (NEB HiFi Assembly Kit).

405 Oligos containing a 3xFLAG sequence were annealed by incubation in standard annealing buffer
406 (10 mM Tris-HCl pH 7.5, 1 mM EDTA, 50 mM NaCl) for 5 min at 95°C followed by slow cooling to
407 25°C. The annealed fragment was then digested with BamHI and XhoI and cleaned up by
408 MinElute PCR purification (Qiagen). The eGFP-AID-Usp9x vector was also digested with
409 BamHI/XhoI and cleaned up by gel extraction (Qiagen). The 3xFlag sequence was then ligated
410 into the digested eGFP-Usp9x plasmid (Takara DNA ligation kit #6023).

411

412 **ES cell targeting**

413 Vectors were amplified by transformation into Stbl3 competent cells (Invitrogen). Resultant
414 colonies were picked for miniprep DNA extraction (Qiagen) and screening by restriction enzyme
415 digest. Positive clones were sequence-verified, purified by Maxiprep column extraction (Qiagen),
416 concentrated by standard ethanol precipitation overnight, and used for nucleofection into low
417 passage (p3) *OsTir1*-knockin ES cells derived as described³³. Briefly, this line (148.4) was derived
418 from E14 mouse ES cells and is homozygous for a Tir1-2A-Puro cassette (Addgene plasmid #
419 92142 ; <http://n2t.net/addgene:92142> ; RRID:Addgene_92142) at the *TIGRE* locus.

420

421 5 million *OsTir1* cells (passage 4) were nucleofected with 2.5 µg of the sgRNA plasmid and 20 µg
422 of either eGFP-AID-Usp9x plasmid or eGFP-3xFLAG-Usp9x plasmid, using an Amaxa
423 Nucleofector 2b device and ES nucleofection kit (Lonza) per the manufacturer's instructions. Cells
424 were diluted in 500 µl of medium and immediately plated onto 10 cm dishes with 10 ml pre-
425 warmed medium. After 2 days, GFP-single and BFP-/GFP-double-positive cells were sorted by
426 FACS and plated at clonal density (10,000 cells per 10cm dish). Clones were left to expand for 5
427 days before manual picking onto 96-well plates. Single clones were then dissociated and
428 expanded for 2 days. Clones were screened for auxin responsiveness by replica plating onto 2
429 96w plates, addition of auxin to 1 plate, and measurement of eGFP fluorescence intensity by flow
430 cytometry. Auxin-responsive clones were subsequently expanded and used as biological
431 replicates for all analyses. Cells were periodically pulsed with puromycin (1 µg/ml for 1-2 days) to
432 select against transgene silencing.

433

434 **Usp9x-CD-mCherry cloning**

435 The Usp9x catalytic domain was amplified from a plasmid containing the full-length Usp9x ORF,
436 obtained from DNASU⁹⁸; mCherry was amplified by PCR from a pcDNA3-mCherry plasmid. We
437 then cloned the purified Usp9x-DUB and mCherry fragments into pEF1a-IRES-Neo, a gift from
438 Thomas Zwaka (Addgene plasmid # 28019; <http://n2t.net/addgene:28019>;

439 RRID:Addgene_28019), by Gibson Assembly. To make the C1566S catalytic mutant form of the
440 Usp9x DUB domain, we performed site directed mutagenesis⁹⁹. PCR was carried out with
441 Phusion polymerase (New England Biolabs), with PCR cycling conditions: 98°C for 7 min; 12
442 cycles of 98°C for 30s, 61°C for 30s, 72°C for 3 min 45s; 3 cycles of 98°C for 30s, 56°C for 30s,
443 72°C for 3m 45s; 72°C for 10 min; 4°C hold. The PCR product was digested with DpnI for 3h at
444 37°C (New England Biolabs) and then 5 µl was transformed into Stbl3 competent cells (Thermo
445 Fisher Scientific). See Supplementary Table 3 for primer sequences.

446

447 **Mouse embryonic stem cell culture**

448 ES cells were passaged every 1-2 days and grown in standard ES-FBS (serum/LIF) medium:
449 DMEM GlutaMAX with Na Pyruvate, 15% fetal bovine serum (Atlanta Biologicals, GA, USA), 0.1
450 mM Non-essential amino acids, 50 U/ml Penicillin/Streptomycin, 0.1 mM EmbryoMax 2-
451 Mercaptoethanol and 1000 U/ml ESGRO supplement. Cells tested negative for Mycoplasma
452 contamination.

453

454 Indole-3-acetic acid sodium salt (Sigma I5148-2G) was dissolved in water to 500 mM, filter
455 sterilized, and stored as aliquots at -20°C. Stock solutions were thawed and diluted to 500 µM for
456 all depletion experiments. Wild-type ES cells were used to determine the range of GFP-negative
457 expression for sorting Usp9x-low ES cells upon auxin treatment. Usp9x-low and Usp9x-high cells
458 correspond to the bottom and top ~15-20% of the population by GFP expression, respectively.

459

460 **Embryonic stem cell differentiation**

461 LIF was withdrawn from ES-FBS medium for spontaneous differentiation into Embryoid Bodies
462 (EB). ES cells were counted, plated on low-attachment 6w plates, and harvested by trypsinization
463 at day 2 and day 5 for qRT-PCR or western blot analysis.

464

465 **siRNA-mediated Knockdown**

466 siRNA transfections were performed in ES cells using Lipfectamine 2000 and OptiMEM (Thermo
467 Fisher Scientific). ES cells were plated 5-7h before transfection at a density of 5×10^5 cells per
468 well of a 6-well plate and transfected with 100 pmol siRNA, according to the manufacturer's
469 standard recommendations. A SMARTpool of 4 independent siRNAs were used to knock down
470 Usp9x (Dharmacon), and a non-targeting siRNA (siGenome siControl #2, Dharmacon) was used
471 as a control. Transfections were performed in ES-FBS medium without antibiotics, and the

472 medium was replaced the next morning with complete ES-FBS. Cells were harvested for counting
473 and colony formation assays or western blots 48h after transfection.

474

475 **Colony formation assay**

476 1000 cells from the indicated conditions were sorted and plated onto a 12-well plate. 4 replicates
477 were performed for 2 independent sorts. Cells were grown in self-renewal conditions (serum/LIF)
478 for 5-6 days. Colonies were then washed 1x in PBS, fixed for 15 minutes at RT in 2% PFA, and
479 stained according to the instructions of the VectorRed Alkaline Phosphatase (AP) Substrate Kit
480 (Vector Laboratories, CA, USA). Colonies were manually scored based on colony morphology
481 and AP staining (positive if >50% of colony area).

482

483 **qRT-PCR**

484 cDNA synthesis was performed with the High-Capacity cDNA Reverse Transcription Kit (Thermo
485 Fisher Scientific), using random hexamer priming for 2 hours at 37°C. KAPA 2x SYBR Green
486 Master Mix, low ROX (KAPA) was used for qPCR and data were acquired on a QuantStudio 5
487 (Thermo Fisher Scientific) and analyzed in Prism v8 (GraphPad).

488

489 **RNA-seq library preparation**

490 3 independent clones of each cell line (AID-Usp9x or Flag-Usp9x) were used for RNA-
491 sequencing. Cells were plated the day before sorting, and auxin was added to a final
492 concentration of 500 μ M in fresh media for 8h. Cells were collected by trypsinization and
493 resuspended in FACS buffer (10% FBS, PBS, \pm 500 μ M auxin) with SYTOX Blue (Thermo Fisher
494 Scientific) for sorting. 250,000 cells from each condition were sorted on the basis of negative
495 SYTOX Blue incorporation. For the 8h timepoint, sorted cells were immediately pelleted,
496 resuspended in Buffer RLT + β -mercaptoethanol (Qiagen), snap frozen on dry ice, and stored at
497 -80°C before library preparation. For the 48h recovery timepoint, cells were re-plated in regular
498 ES-FBS medium, cultured for 48h in serum/LIF without auxin, lysed, and snap frozen. Sorts were
499 performed on a Sony SH800 Single Cell Sorter (Sony).

500

501 RNA extractions from frozen lysates were performed on the same day using RNeasy Mini columns
502 (Qiagen). Recovered total RNA was quantified by Qubit and quality was assessed using an
503 Agilent Bioanalyzer, RNA pico kit (Agilent). Synthetic RNAs from the External RNAs Control
504 Consortium (ERCC) Spike-in Mix1 (Thermo Fisher Scientific) were added at known
505 concentrations to the same volume of RNA from the previous step, per manufacturer's instructions

506 (2 μ l of 1:100 ERCC dilution added to 10 μ l of RNA, representing \sim 1-1.5 μ g RNA). 1 μ g of total
507 RNA was used for mRNA isolation and library preparation using the NEBNext Ultra II Directional
508 Library Prep Kit for Illumina with the mRNA Magnetic Isolation Module, per manufacturer's
509 instructions (New England Biolabs, NEB #E7420S and #E7490S). Library quality was assessed
510 by Bioanalyzer High Sensitivity DNA chip (Agilent). Libraries were quantified by Qubit and pooled
511 at equimolar concentration. Sequencing was performed on a HiSeq 4000 (Illumina) with 50 bp
512 single-end reads at the UCSF Center for Advanced Technology.

513

514 For embryo RNA-seq, whole E8.5 embryos were dissected, cleaned of extraembryonic tissue,
515 resuspended in buffer RLT + β -mercaptoethanol (Qiagen), and snap-frozen on dry ice. 3 litter-
516 matched control and mutant embryos were collected from 2 litters, for a total of $n = 12$ individual
517 embryos. RNA was extracted as above and 300 ng of total RNA was used for library preparation
518 using the NEBNext Ultra II Directional Library Prep Kit for Illumina with the mRNA isolation module
519 and NEBNext Multiplex Oligos for Illumina (New England Biolabs). DNA quality was assessed by
520 Fragment Analyzer NGS (Agilent). Libraries were quantified by Qubit and pooled at equimolar
521 concentration for sequencing on a NextSeq 500 (Illumina) with 75 bp single-end reads at the LTRI
522 Sequencing Core.

523

524 **RNA-seq analysis**

525 Libraries were trimmed of Illumina adaptor sequences and quality-checked using Trim Galore!
526 (Babraham Bioinformatics), and then aligned to the mm10 transcriptome with ERCC sequences
527 using TopHat2 v2.0.13 options -g 20 --no-coverage-search --library-type fr-firststrand --no-novel-
528 indels¹⁰⁰. Gene counts were obtained from featureCounts on the command line with options: -t
529 exon -T 8 -s 2 -g gene_id. The table of raw counts was imported into R, filtered to remove low-
530 count genes (genes with 0 counts in any sample and those with ≤ 3 counts per million, CPM by
531 edgeR, across all samples were filtered out), and separated into ERCC and gene counts. Values
532 for spike-in normalization were determined from ERCC counts corrected for overall library size
533 using edgeR calcNormFactors (nf <- calcNormFactors(raw_ercc_counts, lib.size=N), where N <-
534 colSums(raw_gene_counts). The CNN factors were then used to adjust gene counts using the
535 limma-voom transformation (option lib.size = N*nf)¹⁰¹. Data were further analyzed and plotted
536 using ggplot2. The threshold for significant differential expression was adjusted $P < 0.05$ and
537 $\log_2FC > |0.7|$ relative to control cells (AID-Usp9x without auxin and Flag-Usp9x). Boxplots and
538 violin plots show fold-change relative to control cells obtained from toptable analyses.

539 For embryo RNA-seq, gene counts were obtained in the same manner, imported into R, and
540 converted to a DESeq2 object (DESeqDataSetFromMatrix using sample information) for
541 processing, DESeq2 version 1.24.0¹⁰². Genes with fewer than 10 counts across all samples were
542 filtered out before differential expression analysis. Counts normalized by the DESeq2 rlog
543 transformation were used for PCA and heatmaps of gene expression. Raw counts were used for
544 differential expression analysis using the default parameters of the DESeq function. To account
545 for staging differences between litters, we called differential expression between litter-matched
546 mutants and controls, applied a statistical cutoff (adjusted $P < 0.1$), and overlapped the gene lists
547 to obtain refined sets of up- or down-regulated genes. RNA-seq data from post-occipital embryos
548 stages E6.5, E7.8, and E8.5 are from⁵⁶. Published DESeq2 results were used to plot fold-changes
549 in expression from E6.5, and raw fastq files were downloaded from NCBI GEO, converted to
550 normalized gene counts as above, and used to plot Nodal expression.

551

552 **Gene Ontology analyses**

553 Pathway analysis was performed by Gene Ontology (GO) analysis using DAVID 6.8 and
554 geneontology.org^{103–106}. Transcription factor binding enrichment of gene lists was performed with
555 ChEA, part of the Enrichr suite (<https://amp.pharm.mssm.edu/Enrichr/>)^{42,107}. Tables of enriched
556 factors and P-values were downloaded and plotted in R.

557

558 Gene Set Enrichment Analysis (GSEA v6.0.12) was performed using the online GSEAPreranked
559 tool (<https://cloud.genepattern.org/gp/pages/login.jsf>) with default conditions to compare
560 differential expression (all genes sorted by log₂FC) with gene sets from published datasets,
561 outlined below³⁴. Normalized enrichment scores were plotted in Prism v8 (GraphPad).

562

563 *Datasets used for GSEA*

564 The 2-cell embryo signature is from¹⁰⁸. Transcriptional signatures from cleavage stages through
565 E5.5 were retrieved from³⁶, taking either the full gene list or the top 500 genes enriched for a
566 particular time point from the published stage-specific expression analysis. The E6.5 epiblast
567 signature was defined as genes upregulated in E6.5 epiblast relative to visceral endoderm and
568 endoderm at E6.5³⁷. A signature of early mesoderm was determined from published RNA-seq of
569 ES cell differentiation, and we selected genes by fold-change of expression at the mesoderm
570 stage compared to ES cells¹⁰⁹. The endoderm signature comes from published microarray data
571 of early endoderm in E7.5 embryos¹¹⁰. Neuroectoderm genes were defined by RNA-seq data of

572 epiblast stem cell differentiation to neural fate, comparing the fold-change in expression at day 2
573 of differentiation relative to baseline¹¹¹. In all cases, either the full published gene list or the top
574 500 genes ranked by fold-change were used for GSEA.

575

576 **Histone extraction**

577 Histone extraction was performed using a standard acid extraction protocol¹¹². Sorted cells were
578 lysed for 10 min at 4°C in triton extraction buffer (PBS with 0.5% Triton X-100, 2 mM PMSF, 1x
579 Halt Protease Inhibitor at a density of 10⁷ cells/ml). Lysates were spun for 10 min at 4°C, 2000
580 rpm. The pellet was washed once in 0.5x volume of lysis buffer and centrifuged again. Pellets
581 were resuspended in 0.2 N HCl (10⁶ cells/ml) and acid extracted overnight, rotating at 4°C. The
582 next day, the solution was clarified by centrifugation and the supernatant transferred to a new
583 tube. Histones were precipitated in 0.25x volume TCA, incubated 20 minutes on ice, and pelleted
584 at max speed for 10 min. Excess acid was removed from solution through two washes in ice-cold
585 acetone, pellets were air-dried, and histones were resuspended in water for BCA Protein
586 quantification (Pierce). LDS sample buffer (Thermo Fisher Scientific) was added to 1x and
587 samples were denatured for 5 min at 95°C followed by cold shock.

588

589 **Co-immunoprecipitations**

590 Co-immunoprecipitation (Co-IP) assays were performed on nuclear extracts. ES cells grown to
591 ~70% confluency were washed twice and then scraped in cold PBS. Cell pellets were weighed
592 and resuspended in 4x volume of swelling buffer A (10 mM HEPES pH 7.9, 5 mM MgCl₂, 0.25 M
593 Sucrose, 0.1% NP-40) with protease inhibitors were added fresh (1x Halt Protease inhibitors, 1
594 mM PMSF, 1 mM NaF, 10 mM N-ethylmaleimide). Lysates were incubated on ice for 20 min and
595 passed through a 18 ½ G needle five times. Nuclei were pelleted by centrifuged for 10 min at
596 1500 g and lysed in 8x volume buffer B (10 mM HEPES pH 7.9, 1 mM MgCl₂, 0.1 mM EDTA, 25%
597 glycerol, 0.5% Triton X-100, 0.5 M NaCl with PIs as in buffer A). After incubation on ice for 10
598 min, samples were passed through an 18 ½ G needle 5 times and pulse sonicated using a probe
599 sonicator, 2 times 5 seconds at 4°C. 100 µl of lysate was diluted in 400 µl IP wash/dilution buffer
600 (150 mM NaCl, 10 mM Tris pH 8, 0.5% sodium deoxycholate, 1% Triton X-100, 1 mM EDTA, 1
601 mM EGTA) and rotated 4h-overnight with 1 µg Rb anti-Usp9x (Bethyl), 1.7 µg Rb anti-Ezh2 (CST
602 #5246), or 1.7 µg Rb anti-IgG (Millipore CS200581). Input samples were collected at this time.
603 Immune complexes were bound by 25 µl of pre-washed Protein A Dynabeads (Thermo Fisher
604 Scientific), rotating end-over-end for 2h at 4°C. Beads were washed in IP wash/dilution buffer, 3x5

605 min at 4°C. Input and IP samples were eluted and denatured by boiling in 2x Laemmli buffer/bME
606 for 10 min at 95°C.

607

608 Co-IPs were also performed using Flag M2-bound magnetic agarose beads (Sigma) and GFP-
609 Trap beads (ChromoTek). For Flag pull-downs, AID-Usp9x ES cell were used as controls for
610 nonspecific binding to the Flag beads. For GFP pull-downs, the same amount of lysate was added
611 to negative beads (ChromoTek) to control for nonspecific binding to beads. Cells were collected
612 as above but diluted into GFP-Trap dilution buffer (10 mM Tris-HCl pH 7.5, 150 mM NaCl, 0.5
613 mM EDTA), immunoprecipitated by rotating for 1.5h at 4°C, and washed by 3x fast washes in
614 GFP-Trap dilution buffer. Input and IP samples were denatured as above.

615

616 **HA-Ubiquitin Immunoprecipitations**

617 HA-tagged ubiquitin (a gift of the F. Sicheri lab) was overexpressed in ES cells by transfection
618 with Lipofectamine 2000 (Thermo Fisher Scientific), 500 ng per $\sim 8 \times 10^6$ cells in a 10 cm dish.
619 Water diluted in Lipofectamine was used for mock transfections. Medium was changed the next
620 morning and cells were harvested after 24 hours. Adherent cells were washed twice and then
621 scraped into cold PBS. The resulting cell pellets were weighed and resuspended in 4x volume of
622 RIPA buffer (150 mM NaCl, 1% NP-40, 0.5% Na deoxycholate, 0.1% SDS, 50 mM Tris pH 8) to
623 lyse for 15 min on ice. Pellets were centrifuged at max speed for 10 min at 4°C to remove insoluble
624 material. 100 μ l of supernatant was taken for IP and diluted to 500 μ l in non-denaturing lysis buffer
625 (20 mM Tris pH 8, 137 mM NaCl, 1% Triton X-100, 2 mM EDTA) plus 2.5 μ g of anti-HA antibody
626 (Abcam ab9110). IPs were incubated overnight at 4°C with end-over-end rotation. The next day,
627 immune complexes were bound to 25 μ l Protein A Dynabeads (Thermo Fisher Scientific) for 2h
628 at 4°C. Complexes were washed on beads for 3x10 min in IP wash buffer (150 mM NaCl, 10 mM
629 Tris pH 8, 0.5% Na deoxycholate, 1% Triton X-100, 1 mM EDTA, 1 mM EGTA) and eluted in 2x
630 Laemmli buffer/10% β -mercaptoethanol for 10 min at 95°C followed by cold shock on ice. Input
631 samples were collected and denatured in Laemmli buffer to 1x. Samples were removed from
632 beads for western blotting.

633

634 For Usp9x catalytic domain expressions, transfections were performed as above but with the
635 addition of 2.5 μ g of plasmid (wild-type or C1566S pEF1a-Usp9x_CD-mCherry) and in medium
636 without Pen/Strep. Transfection was checked by mCherry fluorescence the next morning. IPs
637 were performed as above but with the following antibodies instead of HA: Ezh2 at 1:300 (CST
638 #5246), Suz12 at 1:50 (CST #3737), or rabbit IgG at 1:50 (Millipore CS200581).

639

640 **Subcellular fractionation**

641 Subcellular fractionation was performed as previously reported¹¹³. Cell pellets were resuspended
642 in buffer A (10 mM HEPES pH 7.9, 10 mM KCl, 1.5 mM MgCl₂, 0.34M sucrose, 10% glycerol,
643 0.1% Triton X-100, 1 mM DTT, and PIs: NaF, PMSF, 1x Halt Protease inhibitor cocktail),
644 incubated 5 min on ice, and centrifuged for 5 min at 1300 *g* at 4°C. The supernatant was taken
645 as the cytoplasmic extract and clarified by centrifugation. Nuclear pellets were washed in buffer
646 A and resuspended in buffer B (3 mM EDTA, 0.2 mM EGTA, 1 mM DTT, and PIs). After 5 min on
647 ice, chromatin pellets were centrifuged for 5 min at 1700 *g*, 4°C. The supernatant was collected
648 as the soluble nucleoplasmic fraction. Insoluble pellets were resuspended in 1x Laemmli buffer
649 containing 5% β-mercaptoethanol and sonicated on a Bioruptor: high power, 30s on, 30s off, 5
650 min total (Diagenode).

651

652 **Western blot analysis**

653 Denatured samples were separated on 4-15% Mini-Protean TGX SDS-PAGE gels (Bio-rad).
654 Protein was transferred to methanol-activated PVDF membranes (Bio-rad) by wet transfer (1x
655 Pierce Transfer Buffer, 10% methanol) or using high molecular weight transfer conditions for the
656 Bio-rad TransBlot Turbo (Bio-rad). Membranes were blocked in 5% milk/TBS-T and incubated
657 with indicated primary antibodies for 1.5h at room temperature or overnight at 4°C. Membranes
658 were then washed and incubated with HRP-conjugated anti-mouse/rabbit secondary antibodies
659 (Jackson Labs) for 1h at room temperature. Proteins were detected by ECL (Pierce) or Clarity
660 (Bio-rad) detection reagents and exposure to X-ray film (Pierce).

661

662 For analysis of cell cycle, Fucci reporter ES cells³³ were collected by trypsinization and sorted
663 on a FACS AriaII (BD Biosciences) into mCherry+ (G0/G1) and BFP+ (S/G2/M) cell fractions.
664 Cells were pelleted and lysed in RIPA buffer and clarified by centrifugation for 10 min, 13,000 *g*
665 at 4°C. Lysates from the same number of cells were used for western blotting.

666

667 **H3K27me3 ChIP-seq**

668 Two biological replicates, consisting of independent clones of AID-Usp9x collected on
669 consecutive days, were collected. 10⁶ cells were sorted and cross-linked in 1%
670 formaldehyde/PBS, rotating for 10 min at room temperature. Cross-links were quenched with
671 glycine (125 mM final) for 5 min at room temperature. Cells were washed 2x in cold PBS, snap
672 frozen, and stored at -80°C. All subsequent steps were performed on ice or at 4°C. Fixed cell

673 pellets were thawed and lysed in 1% SDS, 10 mM EDTA, 50 mM Tris-HCl pH 8 with protease
674 inhibitors (1x Halt Protease inhibitor cocktail, 1 mM PMSF, 1 mM NaF) for 30 min. Chromatin was
675 sheared to 200-500 bp fragments on a Covaris S220 with settings PIP 105, duty 2, cpb 200 for 9
676 min. Shearing efficiency was confirmed by 1% agarose gel electrophoresis. Chromatin lysates
677 were clarified by centrifugation and diluted 1:10 in dilution buffer (1% Triton X-100, 2 mM EDTA,
678 167 mM NaCl, 20 mM Tris-HCl pH 8) with protease inhibitors. Inputs were collected at the same
679 time. IPs were performed overnight using 2.5 µg of antibody (CST #9733 H3K27me3 or Abcam
680 ab46540 rabbit IgG) per equivalent of 500,000 cells, rotating at 4°C. The next day,
681 immunocomplexes were precipitated by incubation with pre-washed Protein A Dynabeads
682 (Invitrogen) for 2h. Beads were washed 4x10 min in low-salt buffer (0.1% SDS, 1% Triton X-100,
683 2 mM EDTA, 150 mM NaCl, 20 mM Tris-HCl pH 8), 1x10 min in high-salt buffer (0.1% SDS, 1%
684 Triton X-100, 2mM EDTA, 500 mM NaCl, 20 mM Tris-HCl pH 8), 1x10 min in LiCl buffer (0.25 M
685 LiCl, 0.5% NP-40, 0.5% Na deoxycholate, 1 mM EDTA, 10 mM Tris-HCl pH 8), and 1x fast in TE.
686 CHIP and input samples were eluted in fresh CHIP elution buffer (1% SDS, 50 mM NaHCO₃, 50
687 mM Tris-HCl pH 8, 1 mM EDTA) and treated with RNase A for 1h at 37°C. Cross-links were
688 reversed by shaking overnight at 65°C with Proteinase K.

689
690 Genomic DNA was cleaned up using Qiagen MinElute Reaction Cleanup Kit (Qiagen) and
691 quantified by Qubit (Thermo Fisher Scientific). CHIP efficiency was confirmed by H3K27me3
692 enrichment relative to IgG IP in qPCR at diagnostic regions. The same amount of chromatin from
693 HEK293 cells was spiked in to equivalent volumes of CHIP eluates (62 pg of spike-in chromatin
694 per 25 µl of CHIP), yielding final concentrations between ~1-5%. Libraries were constructed from
695 2.5 ng of DNA and prepared using the NEBNext Ultra II DNA Library Prep Kit for Illumina with 9
696 PCR cycles (NEB #E7645S, New England Biolabs). Library quality was assessed by High
697 Sensitivity DNA Assay on an Agilent 2100 Bioanalyzer (Agilent Technologies). Samples were
698 sequenced on a HiSeq 4000 using single-end 50 bp reads.

699

700 **H3K27me3 ChIP-seq data analysis**

701 Sequencing reads that passed quality control were trimmed of adaptors using Trim Galore! v0.4.0
702 and aligned to mm10 and hg19 using bowtie2 v2.2.5¹¹⁴ with no multimapping. SAM files were
703 converted to BAM files, sorted, and indexed. Normalization factors (NFs) for each sample were
704 calculated as a fraction of input reads⁸. Bam files were deduplicated using picard v2.18.14
705 MarkDuplicates (<http://broadinstitute.github.io/picard>). Raw H3K27me3 ChIP-seq data were
706 downloaded as fastq files from NCBI GEO for the indicated datasets. For paired-end samples,

707 only one read was kept per fragment and all samples were trimmed, aligned to mm10, sorted,
708 and deduplicated as above. Deduplicated bam files were analyzed using deepTools v3.3.0 on the
709 command line¹¹⁵. Library sizes for normalization were calculated from bam files before
710 deduplication (samtools view -c).

711

712 *Broad peak calling*

713 Deduplicated bam files were converted to scaled bedgraphs using deepTools bamCoverage
714 (options --scaleFactor <NF> --binSize 10 --blackListFileName ENCODE_mm10_blacklist.bed)
715 and then to bed files: awk '{print \$1"\t"\$2"\t"\$3"\tid-"NR"\t"\$4"\t."}'. These scaled bed files were
716 used to call broad peaks compared to input using epic2 on the command line (options -gn mm10,
717 -d chrM). Bedtools merge was used to merge peaks within 3kb, and bedtools intersect was used
718 to determine a set of common peaks between replicates. Bam files were converted to scaled
719 bigWigs using deepTools bamCoverage (options --binSize 100 --scaleFactor <NF>). Correlation
720 between replicates was checked by multiBigWigSummary bins and plotCorrelation, and then
721 scaled bw files were merged (bigwigCompare add) for heatmaps. computeMatrix was used to
722 generate coverage of scaled bigwig files over no-auxin peaks (options scale-regions -m 500 --
723 upstream 10000 --downstream 10000 --binSize 100 --missingDataAsZero --skipZeros --
724 sortRegions descend --sortUsing mean --sortUsingSamples 1 -p max). Heatmaps were produced
725 using deepTools plotHeatmap.

726

727 TSS profile plots were generated from the output of deeptools plotProfile (--outFileNameData),
728 which was imported into R, processed to average replicates, and then plotted with ggplot2. For
729 H3K27me3 coverage over *Nodal*, bigwig files were downloaded from NCBI GEO⁵⁸. Sample tracks
730 were visualized in Integrated Genome Viewer using bigwig files (IGV v2.3.92).

731

732 multiBamSummary was used to count reads falling into non-overlapping 10kb genes across the
733 genome, and read counts were then imported into R. Embryo counts were normalized by library
734 sizes (number of mapped reads in deduplicated bam files), and ES cell data were normalized by
735 spike-in factors. For cumulative distribution plots, reads were counted in non-overlapping 10kb
736 genomic bins using deeptools multiBamSummary (options --smartLabels --blackListFileName --
737 outRawCounts --minMappingQuality 10 -p max). The resulting counts table was imported into R,
738 filtered to remove regions without coverage, scaled with the NFs calculated above, and then
739 plotted using ggplot2 (stat_ecdf). P-values represent Kolmogorov-Smirnov test results using the

740 averages of biological replicates. Counts per bin were adjusted for biological batch (embryo vs.
741 ES cell origin) using ComBat/sva in R¹¹⁶ and analyzed by PCA.

742

743 For analysis of repetitive elements, H3K27me3 was counted over repetitive elements annotated
744 in the mouse genome (obtained from UCSC RepeatMasker) using featureCounts (options -f -O -
745 s 0 -T 8). In R, we filtered out elements with low coverage, scaled using the NFs calculated above,
746 and calculated the average of replicates. Plots show regions with > 5 normalized counts for hyper-
747 H3K27me3 and < 3 for hypo-H3K27me3 elements, with $\log_2(\text{Usp9x-high/no-auxin}) > |0.7|$ as the
748 threshold for enrichment.

749 **REFERENCES**

- 750
- 751 1. Ying, Q.-L. *et al.* The ground state of embryonic stem cell self-renewal. *Nature* **453**, 519–523
752 (2008).
- 753 2. Blaschke, K. *et al.* Vitamin C induces Tet-dependent DNA demethylation and a blastocyst-like
754 state in ES cells. *Nature* **500**, 222–226 (2013).
- 755 3. Boroviak, T., Loos, R., Bertone, P., Smith, A. & Nichols, J. The ability of inner-cell-mass cells
756 to self-renew as embryonic stem cells is acquired following epiblast specification. *Nature Cell*
757 *Biology* **16**, 513–525 (2014).
- 758 4. Bulut-Karslioglu, A. *et al.* Inhibition of mTOR induces a paused pluripotent state. *Nature* **540**,
759 119–123 (2016).
- 760 5. Bulut-Karslioglu, A. *et al.* The Transcriptionally Permissive Chromatin State of Embryonic
761 Stem Cells Is Acutely Tuned to Translational Output. *Cell Stem Cell* **22**, 369–383.e8 (2018).
- 762 6. Gökbuget, D. & Blelloch, R. Epigenetic control of transcriptional regulation in pluripotency and
763 early differentiation. *Development* **146**, dev164772–16 (2019).
- 764 7. Zheng, H. *et al.* Resetting Epigenetic Memory by Reprogramming of Histone Modifications in
765 Mammals. *Molecular Cell* **63**, 1066–1079 (2016).
- 766 8. Mierlo, G. van *et al.* Integrative Proteomic Profiling Reveals PRC2-Dependent Epigenetic
767 Crosstalk Maintains Ground-State Pluripotency. *Cell Stem Cell* **24**, 123–137.e8 (2019).
- 768 9. Kumar, B. & Elsässer, S. J. Quantitative Multiplexed ChIP Reveals Global Alterations that
769 Shape Promoter Bivalency in Ground State Embryonic Stem Cells. *Cell Reports* **28**, 3274-
770 3284.e5 (2019).
- 771 10. Xiang, Y. *et al.* Epigenomic analysis of gastrulation identifies a unique chromatin state for
772 primed pluripotency. *Nat Genet* **52**, 95–105 (2020).
- 773 11. Azuara, V. *et al.* Chromatin signatures of pluripotent cell lines. *Nat Cell Biol* **8**, 532–538
774 (2006).
- 775 12. Bernstein, B. E. *et al.* A Bivalent Chromatin Structure Marks Key Developmental Genes in
776 Embryonic Stem Cells. *Cell* **125**, 315–326 (2006).
- 777 13. Ramalho-Santos, M., Yoon, S., Matsuzaki, Y., Mulligan, R. C. & Melton, D. A. ‘Stemness’:
778 transcriptional profiling of embryonic and adult stem cells. *Science* **298**, 597–600 (2002).
- 779 14. Blanpain, C., Lowry, W. E., Geoghegan, A., Polak, L. & Fuchs, E. Self-Renewal,
780 Multipotency, and the Existence of Two Cell Populations within an Epithelial Stem Cell Niche.
781 *Cell* **118**, 635–648 (2004).
- 782 15. Jolly, L. A., Taylor, V. & Wood, S. A. USP9X Enhances the Polarity and Self-Renewal of
783 Embryonic Stem Cell-derived Neural Progenitors. *Mol Biol Cell* **20**, 2015–2029 (2009).

- 784 16. Stegeman, S. *et al.* Loss of Usp9x Disrupts Cortical Architecture, Hippocampal
785 Development and TGF β -Mediated Axonogenesis. *PLoS ONE* **8**, e68287-12 (2013).
- 786 17. Oishi, S. *et al.* Usp9x-deficiency disrupts the morphological development of the postnatal
787 hippocampal dentate gyrus. *Sci Rep-uk* **6**, 25783 (2016).
- 788 18. Premarathne, S., Murtaza, M., Matigian, N., Jolly, L. A. & Wood, S. A. Loss of Usp9x
789 disrupts cell adhesion, and components of the Wnt and Notch signaling pathways in neural
790 progenitors. *Sci Rep-uk* **7**, 8109 (2017).
- 791 19. Naik, E. *et al.* Regulation of proximal T cell receptor signaling and tolerance induction by
792 deubiquitinase Usp9X. *The Journal of Experimental Medicine* **211**, 1947–1955 (2014).
- 793 20. Agrawal, P., Chen, Y. T., Schilling, B., Gibson, B. W. & Hughes, R. E. Ubiquitin-specific
794 Peptidase 9, X-linked (USP9X) Modulates Activity of Mammalian Target of Rapamycin (mTOR).
795 *Journal of Biological Chemistry* **287**, 21164–21175 (2012).
- 796 21. Khan, O. M. *et al.* The deubiquitinase USP9X regulates FBW7 stability and suppresses
797 colorectal cancer. *Journal of Clinical Investigation* **128**, 1326–1337 (2018).
- 798 22. Homan, C. C. *et al.* Mutations in USP9X Are Associated with X-Linked Intellectual Disability
799 and Disrupt Neuronal Cell Migration and Growth. *The American Journal of Human Genetics* **94**,
800 470–478 (2014).
- 801 23. Reijnders, M. R. F. *et al.* De Novo Loss-of-Function Mutations in USP9X Cause a Female-
802 Specific Recognizable Syndrome with Developmental Delay and Congenital Malformations. *The*
803 *American Journal of Human Genetics* **98**, 373–381 (2016).
- 804 24. Johnson, B. V. *et al.* Partial Loss of USP9X Function Leads to a Male Neurodevelopmental
805 and Behavioral Disorder Converging on Transforming Growth Factor β Signaling. *Biol Psychiat*
806 **87**, 100–112 (2019).
- 807 25. Jones, M. H. *et al.* The Drosophila developmental gene fat facets has a human homologue
808 in Xp11.4 which escapes X-inactivation and has related sequences on Yq11.2. *Human*
809 *Molecular Genetics* **5**, 1695–1701 (1996).
- 810 26. Tarpey, P. S. *et al.* A systematic, large-scale resequencing screen of X-chromosome coding
811 exons in mental retardation. *Nat Genet* **41**, 535–543 (2009).
- 812 27. Paemka, L. *et al.* Seizures are regulated by ubiquitin-specific peptidase 9 X-linked (USP9X),
813 a de-ubiquitinase. *PLoS Genetics* **11**, e1005022 (2015).
- 814 28. Murtaza, M., Jolly, L. A., Gecz, J. & Wood, S. A. La FAM fatale: USP9X in development and
815 disease. *Cellular and Molecular Life Sciences* **72**, 2075–2089 (2015).
- 816 29. Bailey, M. H. *et al.* Comprehensive Characterization of Cancer Driver Genes and Mutations.
817 *Cell* **173**, 371-385.e18 (2018).

- 818 30. Pérez-Mancera, P. A. *et al.* The deubiquitinase USP9X suppresses pancreatic ductal
819 adenocarcinoma. *Nature* **486**, 266–270 (2012).
- 820 31. Schwickart, M. *et al.* Deubiquitinase USP9X stabilizes MCL1 and promotes tumour cell
821 survival. *Nature* **463**, 103–107 (2010).
- 822 32. Nishimura, K., Fukagawa, T., Takisawa, H., Kakimoto, T. & Kanemaki, M. An auxin-based
823 degron system for the rapid depletion of proteins in nonplant cells. *Nature Methods* **6**, 917–922
824 (2009).
- 825 33. Nora, E. P. *et al.* Targeted Degradation of CTCF Decouples Local Insulation of
826 Chromosome Domains from Genomic Compartmentalization. *Cell* **169**, 930–933.e22 (2017).
- 827 34. Subramanian, A. *et al.* Gene set enrichment analysis: A knowledge-based approach for
828 interpreting genome-wide expression profiles. *Proceedings of the National Academy of*
829 *Sciences* **102**, 15545 (2005).
- 830 35. Kalkan, T. *et al.* Tracking the embryonic stem cell transition from ground state pluripotency.
831 *Development* **144**, 1221–1234 (2017).
- 832 36. Boroviak, T. *et al.* Lineage-Specific Profiling Delineates the Emergence and Progression of
833 Naive Pluripotency in Mammalian Embryogenesis. *Dev Cell* **35**, 366–382 (2015).
- 834 37. Zhang, Y. *et al.* Dynamic epigenomic landscapes during early lineage specification in mouse
835 embryos. *Nat Genet* **50**, 96–105 (2017).
- 836 38. Chambers, I. *et al.* Nanog safeguards pluripotency and mediates germline development.
837 *Nature* **450**, 1230–1234 (2007).
- 838 39. Toyooka, Y., Shimosato, D., Murakami, K., Takahashi, K. & Niwa, H. Identification and
839 characterization of subpopulations in undifferentiated ES cell culture. *Dev* **135**, 909–18 (2008).
- 840 40. Percharde, M., Bulut-Karslioglu, A. & Ramalho-Santos, M. Hypertranscription in
841 Development, Stem Cells, and Regeneration. *Dev Cell* **40**, 9–21 (2017).
- 842 41. Guzman-Ayala, M. *et al.* Chd1 is essential for the high transcriptional output and rapid
843 growth of the mouse epiblast. *Development* **142**, 118–127 (2014).
- 844 42. Kuleshov, M. V. *et al.* Enrichr: a comprehensive gene set enrichment analysis web server
845 2016 update. *Nucleic Acids Res* **44**, W90–W97 (2016).
- 846 43. Pasini, D. *et al.* JARID2 regulates binding of the Polycomb repressive complex 2 to target
847 genes in ES cells. *Nature* **464**, 306–310 (2010).
- 848 44. Leeb, M. *et al.* Polycomb complexes act redundantly to repress genomic repeats and genes.
849 *Genes & Development* **24**, 265–276 (2010).

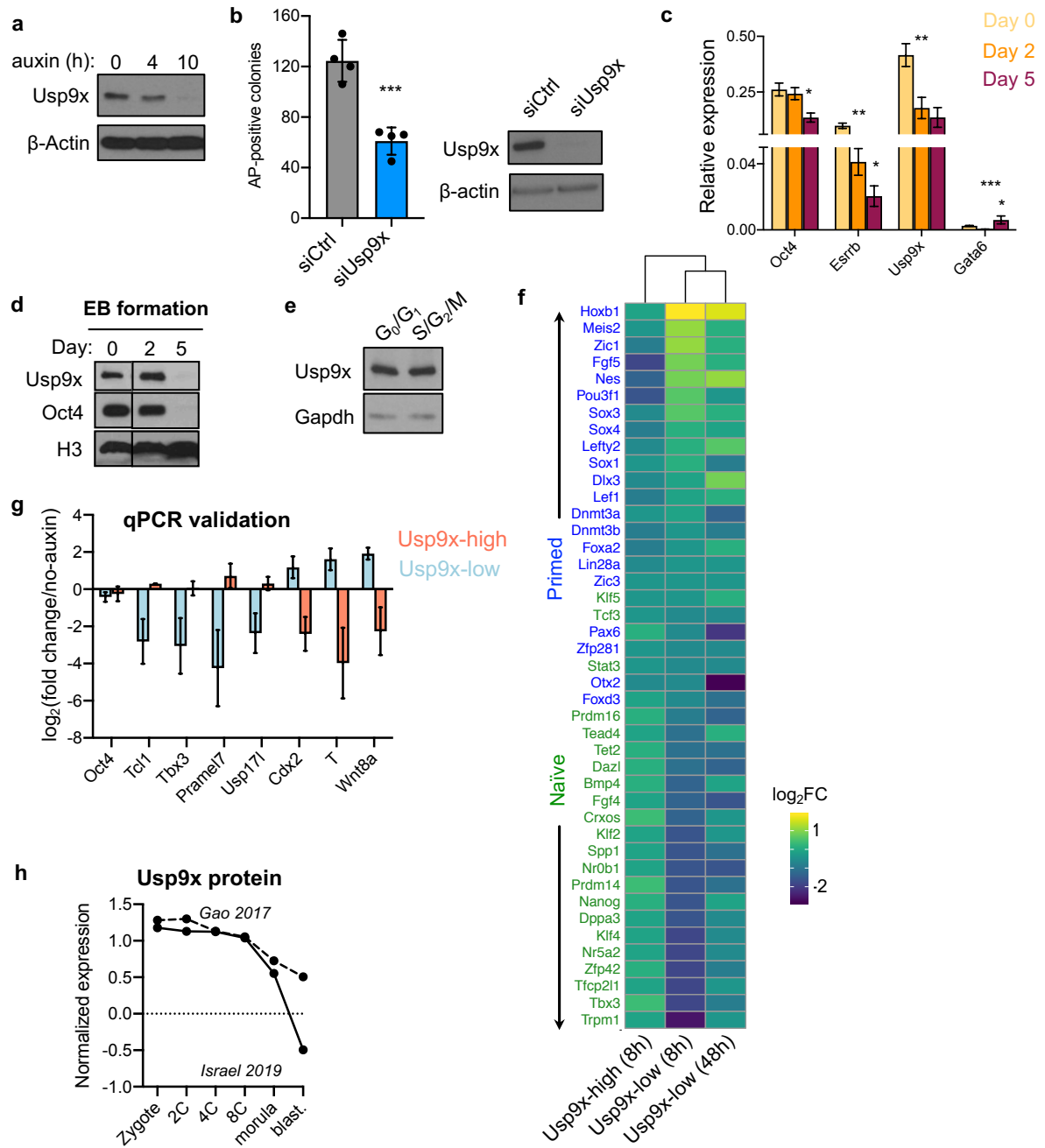
- 850 45. Chamberlain, S. J., Yee, D. & Magnuson, T. Polycomb Repressive Complex 2 Is
851 Dispensable for Maintenance of Embryonic Stem Cell Pluripotency. *Stem Cells* **26**, 1496–1505
852 (2008).
- 853 46. Shan, Y. *et al.* PRC2 specifies ectoderm lineages and maintains pluripotency in primed but
854 not naïve ESCs. *Nature Communications* 1–14 (2017) doi:10.1038/s41467-017-00668-4.
- 855 47. Collinson, A. *et al.* Deletion of the Polycomb-Group Protein EZH2 Leads to Compromised
856 Self-Renewal and Differentiation Defects in Human Embryonic Stem Cells. *Cell Reports* **17**,
857 2700–2714 (2016).
- 858 48. Moody, J. D. *et al.* First critical repressive H3K27me3 marks in embryonic stem cells
859 identified using designed protein inhibitor. *P Natl Acad Sci Usa* **114**, 10125–10130 (2017).
- 860 49. Pasini, D., Bracken, A. P., Hansen, J. B., Capillo, M. & Helin, K. The Polycomb Group
861 Protein Suz12 Is Required for Embryonic Stem Cell Differentiation. *Molecular and Cellular*
862 *Biology* **27**, 3769–3779 (2007).
- 863 50. Nagai, H. *et al.* Ubiquitin-like Sequence in ASK1 Plays Critical Roles in the Recognition and
864 Stabilization by USP9X and Oxidative Stress-Induced Cell Death. *Molecular Cell* **36**, 805–818
865 (2009).
- 866 51. Cox, B. J. *et al.* Phenotypic annotation of the mouse X chromosome. *Genome Res* **20**,
867 1154–1164 (2010).
- 868 52. Pantaleon, M. *et al.* FAM deubiquitylating enzyme is essential for preimplantation mouse
869 embryo development. *Mech Develop* **109**, 151–160 (2001).
- 870 53. Abed, M. *et al.* The Gag protein PEG10 binds to RNA and regulates trophoblast stem cell
871 lineage specification. *PLoS ONE* **14**, e0214110 (2019).
- 872 54. Hayashi, S., Lewis, P., Pevny, L. & McMahon, A. P. Efficient gene modulation in mouse
873 epiblast using a Sox2Cre transgenic mouse strain. *Mech Develop* **119**, S97–S101 (2002).
- 874 55. Wood, S. A. *et al.* Cloning and expression analysis of a novel mouse gene with sequence
875 similarity to the *Drosophila* fat facets gene. *Mech Develop* **63**, 29–38 (1997).
- 876 56. Beccari, L. *et al.* Multi-axial self-organization properties of mouse embryonic stem cells into
877 gastruloids. *Nature* 1–27 (2018) doi:10.1038/s41586-018-0578-0.
- 878 57. Thornton, S. R., Butty, V. L., Levine, S. S. & Boyer, L. A. Polycomb Repressive Complex 2
879 Regulates Lineage Fidelity during Embryonic Stem Cell Differentiation. *PLoS ONE* **9**, e110498-
880 14 (2014).
- 881 58. Wang, C. *et al.* Reprogramming of H3K9me3-dependent heterochromatin during
882 mammalian embryo development. *Nature Cell Biology* 1–23 (2018) doi:10.1038/s41556-018-
883 0093-4.

- 884 59. Marks, H. *et al.* The Transcriptional and Epigenomic Foundations of Ground State
885 Pluripotency. *Cell* **149**, 590–604 (2012).
- 886 60. Walter, M., Teissandier, A., Pérez-Palacios, R. & Bourc'his, D. An epigenetic switch ensures
887 transposon repression upon dynamic loss of DNA methylation in embryonic stem cells. *eLife* **5**,
888 R87 (2016).
- 889 61. Højfeldt, J. W. *et al.* Accurate H3K27 methylation can be established de novo by SUZ12-
890 directed PRC2. *Nature Structural & Molecular Biology* 1–13 (2018) doi:10.1038/s41594-018-
891 0036-6.
- 892 62. Saha, B. *et al.* EED and KDM6B coordinate the first mammalian cell lineage commitment to
893 ensure embryo implantation. *Molecular and Cellular Biology* **33**, 2691–2705 (2013).
- 894 63. Erhardt, S. *et al.* Consequences of the depletion of zygotic and embryonic enhancer of zeste
895 2 during preimplantation mouse development. *Development* **130**, 4235–4248 (2003).
- 896 64. Zhang, M., Wang, F., Kou, Z., Zhang, Y. & Gao, S. Defective Chromatin Structure in
897 Somatic Cell Cloned Mouse Embryos. *J Biol Chem* **284**, 24981–24987 (2009).
- 898 65. Liu, X. *et al.* Distinct features of H3K4me3 and H3K27me3 chromatin domains in pre-
899 implantation embryos. *Nature* **537**, 558–562 (2016).
- 900 66. Kapuria, V. *et al.* Deubiquitinase Inhibition by Small-Molecule WP1130 Triggers Aggresome
901 Formation and Tumor Cell Apoptosis. *Cancer Research* **70**, 9265–9276 (2010).
- 902 67. Oksuz, O. *et al.* Capturing the Onset of PRC2-Mediated Repressive Domain Formation.
903 *Molecular Cell* **70**, 1149-1162.e5 (2018).
- 904 68. Yu, J.-R., Lee, C.-H., Oksuz, O., Stafford, J. M. & Reinberg, D. PRC2 is high maintenance.
905 *Gene Dev* **33**, 903–935 (2019).
- 906 69. Pauler, F. M. *et al.* H3K27me3 forms BLOCs over silent genes and intergenic regions and
907 specifies a histone banding pattern on a mouse autosomal chromosome. *Genome Res* **19**, 221–
908 233 (2009).
- 909 70. Young, M. D. *et al.* ChIP-seq analysis reveals distinct H3K27me3 profiles that correlate with
910 transcriptional activity. *Nucleic Acids Res* **39**, 7415–7427 (2011).
- 911 71. Hawkins, R. D. *et al.* Distinct epigenomic landscapes of pluripotent and lineage-committed
912 human cells. *Cell Stem Cell* **6**, 479–491 (2010).
- 913 72. Carelli, F. N., Sharma, G. & Ahringer, J. Broad Chromatin Domains: An Important Facet of
914 Genome Regulation. *Bioessays* **39**, 1700124 (2017).
- 915 73. Dumesic, P. A. *et al.* Product binding enforces the genomic specificity of a yeast polycomb
916 repressive complex. *Cell* **160**, 204–218 (2015).

- 917 74. Margueron, R. *et al.* Role of the polycomb protein EED in the propagation of repressive
918 histone marks. *Nature* **461**, 762–767 (2009).
- 919 75. Laugesen, A., Højfeldt, J. W. & Helin, K. Molecular Mechanisms Directing PRC2
920 Recruitment and H3K27 Methylation. *Molecular Cell* **74**, 8–18 (2019).
- 921 76. Yap, D. B. *et al.* Somatic mutations at EZH2 Y641 act dominantly through a mechanism of
922 selectively altered PRC2 catalytic activity, to increase H3K27 trimethylation. *Blood* **117**, 2451–
923 2459 (2011).
- 924 77. Sneeringer, C. J. *et al.* Coordinated activities of wild-type plus mutant EZH2 drive tumor-
925 associated hypertrimethylation of lysine 27 on histone H3 (H3K27) in human B-cell lymphomas.
926 *P Natl Acad Sci Usa* **107**, 20980–5 (2010).
- 927 78. McCabe, M. T. *et al.* Mutation of A677 in histone methyltransferase EZH2 in human B-cell
928 lymphoma promotes hypertrimethylation of histone H3 on lysine 27 (H3K27). *Proceedings of the*
929 *National Academy of Sciences of the United States of America* **109**, 2989–2994 (2012).
- 930 79. Inoue, A., Jiang, L., Lu, F., Suzuki, T. & Zhang, Y. Maternal H3K27me3 controls DNA
931 methylation-independent imprinting. *Nature* **547**, 419–424 (2017).
- 932 80. Matoba, S. *et al.* Loss of H3K27me3 Imprinting in Somatic Cell Nuclear Transfer Embryos
933 Disrupts Post-Implantation Development. *Cell Stem Cell* **23**, 343-354.e5 (2018).
- 934 81. Zenk, F. *et al.* Germ line-inherited H3K27me3 restricts enhancer function during maternal-
935 to-zygotic transition. *Science* **357**, 212–216 (2017).
- 936 82. Lee, H.-G., Kahn, T. G., Simcox, A., Schwartz, Y. B. & Pirrotta, V. Genome-wide activities of
937 Polycomb complexes control pervasive transcription. *Genome Res* **25**, 1170–1181 (2015).
- 938 83. Lavarone, E., Barbieri, C. M. & Pasini, D. Dissecting the role of H3K27 acetylation and
939 methylation in PRC2 mediated control of cellular identity. *Nature Communications* 1–16 (2019)
940 doi:10.1038/s41467-019-09624-w.
- 941 84. Rougeot, J. *et al.* Maintenance of spatial gene expression by Polycomb-mediated repression
942 after formation of a vertebrate body plan. *Development* **146**, dev178590-14 (2019).
- 943 85. Akkers, R. C. *et al.* A Hierarchy of H3K4me3 and H3K27me3 Acquisition in Spatial Gene
944 Regulation in *Xenopus* Embryos. *Dev Cell* **17**, 425–434 (2009).
- 945 86. Pasini, D., Bracken, A. P., Jensen, M. R., Denchi, E. L. & Helin, K. Suz12 is essential for
946 mouse development and for EZH2 histone methyltransferase activity. *The EMBO Journal* **23**,
947 4061–4071 (2004).
- 948 87. Faust, C., Schumacher, A., Holdener, B. & Magnuson, T. The eed mutation disrupts anterior
949 mesoderm production in mice. *Development* **121**, 273–285 (1995).
- 950 88. O'Carroll, D. *et al.* The Polycomb-Group Gene *Ezh2* Is Required for Early Mouse
951 Development. *Molecular and Cellular Biology* **21**, 4330–4336 (2001).

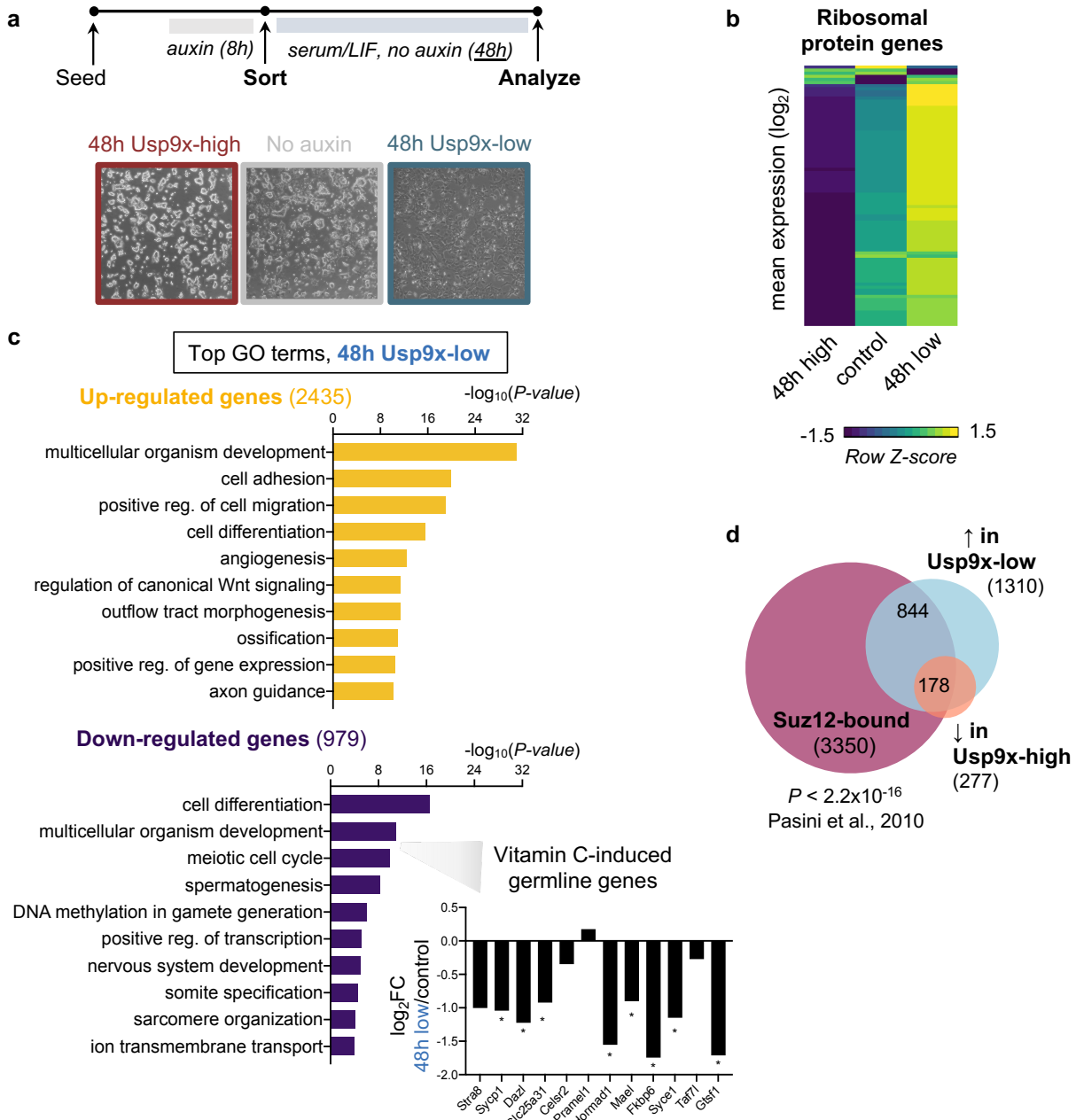
- 952 89. Rugg-Gunn, P. J., Cox, B. J., Ralston, A. & Rossant, J. Distinct histone modifications in
953 stem cell lines and tissue lineages from the early mouse embryo. *Proceedings of the National*
954 *Academy of Sciences of the United States of America* **107**, 10783–10790 (2010).
- 955 90. Yang, X. *et al.* Distinct enhancer signatures in the mouse gastrula delineate progressive cell
956 fate continuum during embryo development. *Cell Research* 1–16 (2019) doi:10.1038/s41422-
957 019-0234-8.
- 958 91. Yang, X. *et al.* Silencing of developmental genes by H3K27me3 and DNA methylation
959 reflects the discrepant plasticity of embryonic and extraembryonic lineages. *Cell Research* 1–4
960 (2018) doi:10.1038/s41422-018-0010-1.
- 961 92. Chiacchiera, F., Rossi, A., Jammula, S., Zanotti, M. & Pasini, D. PRC 2 preserves intestinal
962 progenitors and restricts secretory lineage commitment. *Embo J* **35**, 2301–2314 (2016).
- 963 93. Xie, H. *et al.* Polycomb repressive complex 2 regulates normal hematopoietic stem cell
964 function in a developmental-stage-specific manner. *Cell Stem Cell* **14**, 68–80 (2014).
- 965 94. Boyer, L. A. *et al.* Polycomb complexes repress developmental regulators in murine
966 embryonic stem cells. *Nature* **441**, 349–353 (2006).
- 967 95. Pereira, J. D. *et al.* Ezh2, the histone methyltransferase of PRC2, regulates the balance
968 between self-renewal and differentiation in the cerebral cortex. *Proceedings of the National*
969 *Academy* **107**, (2010).
- 970 96. Rott, R. *et al.* α -Synuclein fate is determined by USP9X-regulated monoubiquitination.
971 *Proceedings of the National Academy of Sciences of the United States of America* **108**, 18666–
972 18671 (2011).
- 973

974 SUPPLEMENTARY FIGURES
975



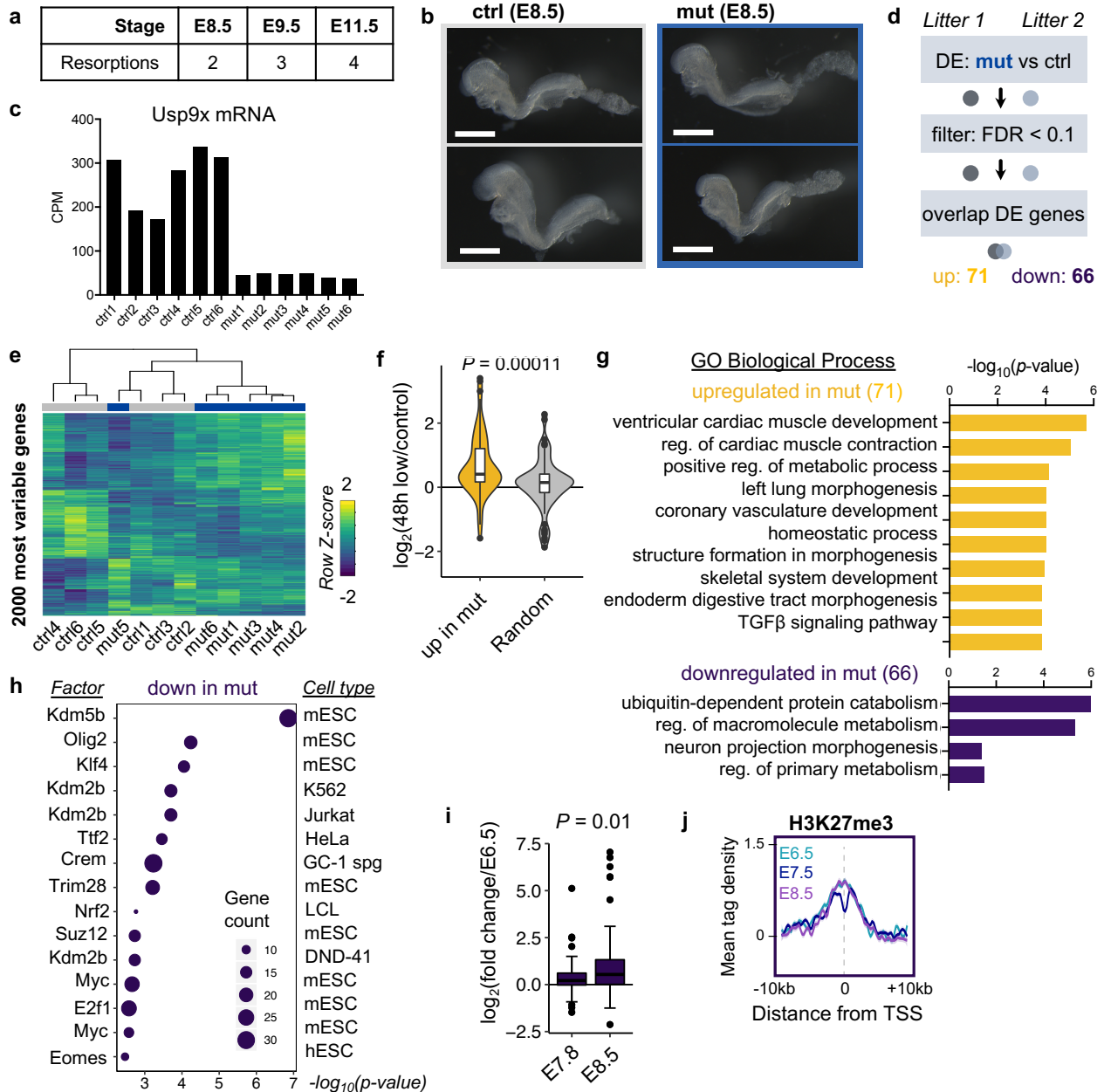
976
977 **Supplementary Figure 1. Characterization of Usp9x expression in targeted ES cells and**
978 **early embryos. a)** Auxin treatment induces acute depletion of endogenous Usp9x protein over a
979 time course of auxin, 0-10h. **b)** Colony formation assay in control (siCtrl) or Usp9x-depleted
980 (siUsp9x) ES cells with western blot confirming Usp9x knockdown. **c)** Usp9x mRNA expression
981 declines during lineage commitment of ES cells in Embryoid Body (EB) formation. **d)** Usp9x
982 protein expression declines during the initial stages of lineage commitment. **e)** Usp9x expression
983 is comparable between stages of the cell cycle, isolated using a Fucci live cell cycle reporter³³.
984 **f)** Relative expression of representative naïve and primed pluripotency genes in the indicated cell

985 states^{4,35}. Data are plotted as \log_2 fold-change (FC) in expression relative to controls. **g**) qRT-
986 PCR validation of representative genes from RNA-seq at 8h after auxin. **h**) Usp9x protein
987 expression declines over pre-implantation development, in parallel with the decline in Usp9x
988 mRNA in early development (Fig. 1e). Normalized data are plotted from quantitative proteomic
989 analyses of wild-type embryos^{117,118}.
990 Data are mean \pm s.d. of 4 replicates and are representative of 3 independent experiments (b),
991 mean \pm SD of 3 replicates (c), mean \pm s.e.m. of 2 biological replicates (g). Western blots are
992 representative of 2-3 biological replicates. * $P < 0.05$, ** $P < 0.01$, *** $P < 0.001$ by Student's t-test
993 (b), multiple t tests with Holm-Sidak correction (c).
994



995
996 **Supplementary Figure 2. Transcriptional analysis of Usp9x-high and Usp9x-low ES cells at**
997 **48h.** **a)** Diagram of experiments assessing the ability of sorted Usp9x-high or Usp9x-low ES cells
998 to recover after acute auxin treatment. After recovery, 48h Usp9x-high ES cells form compact
999 colonies and Usp9x-low ES cells adopt heterogeneous, differentiated morphologies. **b)** Relative
1000 expression of ribosomal protein genes in Usp9x-high, Usp9x-low, or control cells at 48h. **c)** Gene
1001 Ontology (GO) analysis of genes significantly upregulated or downregulated in Usp9x-low ES
1002 cells after 48h. Upregulated genes are enriched for differentiation- and development-related GO
1003 terms. Downregulated genes are enriched for meiosis- and germline-related GO terms,
1004 reminiscent of the hypomethylated state of naïve pluripotency driven by vitamin C addition to 2i
1005 ES cell culture. Inset: \log_2 fold-change (FC) in expression of several vitamin C-induced germline
1006 genes^{2,119}. **d)** Overlap of Suz12-bound genes⁴³ with genes DE in Usp9x-high and Usp9x-low ES

1007 cells (see Fig. 1f). 178 of 248 overlapping DE genes (72%) are Suz12 targets. Boxplot hinges (b)
1008 show the first and third quartiles, with median center line. Data in (c) are the average of 3
1009 replicates. **FDR* < 0.05 or *P* value as indicated. *P*-values by Wilcoxon rank-sum test (b), output
1010 of DESeq2 (c inset), and Fisher exact test (d).

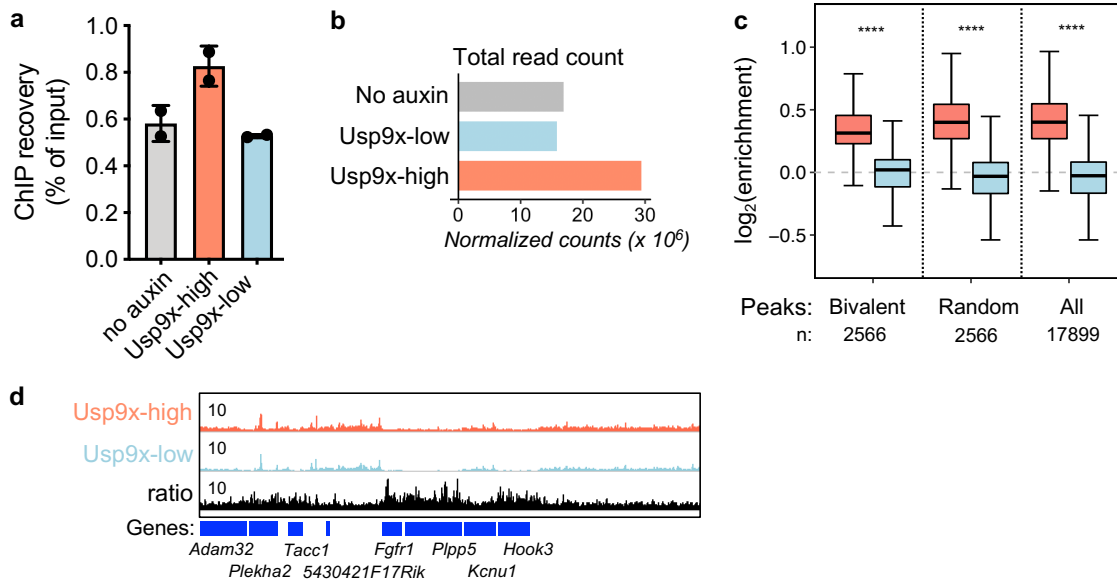


1011
1012
1013
1014
1015
1016
1017
1018
1019
1020
1021
1022

Supplementary Figure 3. Transcriptional analyses of *Usp9x*-mutant embryos at E8.5.

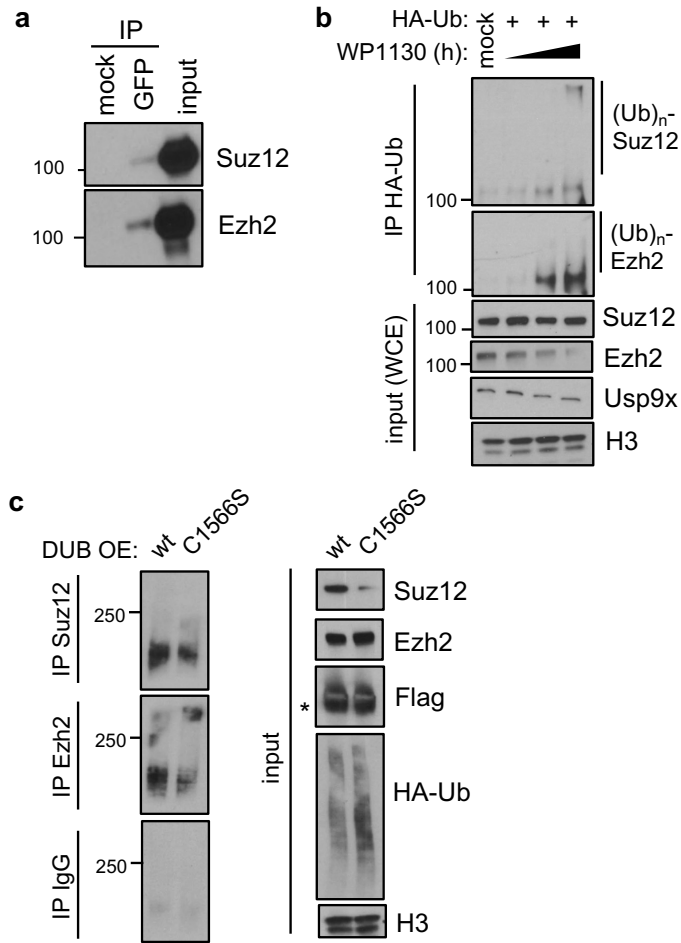
a) Number of resorptions counted at the indicated stages (no embryonic material detected in deciduum). **b**) Representative control and mutant embryos at E8.5 used for RNA-seq. Mutants are morphologically indistinguishable from controls at this stage. Scale bar = 500 μ m. **c**) Normalized counts confirming low *Usp9x* mRNA expression in the 6 mutant embryos used for RNA-seq. $n = 12$ embryos from 2 litters were sequenced. **d**) Approach to DE analysis of E8.5 *Usp9x*-mutant transcriptomes. **e**) Unsupervised hierarchical clustering of the top 2000 most variable genes across samples by RNA-seq. Mutants largely cluster away from controls, except for mut5 (litter 2), which clusters with the controls from litter 1. **f**) Boxplot showing that the genes upregulated in *Usp9x* mutants are also up in 48h *Usp9x*-low ES cells relative to controls,

1023 compared to a random subset of the same number of genes. **g)** Top-enriched GO terms for up-
1024 and down-regulated genes in *Usp9x* mutants. **h)** Enrichr TF analysis of genes downregulated in
1025 *Usp9x*-mutants, similar to Fig. 2e. These genes are targets of repressive chromatin factors, e.g.
1026 Kdm5b, Kdm2b, Trim28, and Suz12, in the indicated cell types. **i)** The genes downregulated in
1027 *Usp9x* mutants tend to be upregulated by E8.5⁵⁶. **j)** Profile of H3K27me3 ChIP-seq signal during
1028 wild-type development over the genes downregulated in *Usp9x* mutants⁵⁸.
1029 Boxplot hinges (f,i) show the first and third quartiles, with median center line. Data are mean \pm
1030 s.e.m. of 2-3 replicates per time point (j). *P* values by Wilcoxon rank-sum test (f, i).



1031
1032
1033
1034
1035
1036
1037
1038
1039
1040
1041
1042

Supplementary Figure 4. Analysis of H3K27me3 patterns in Usp9x-high and Usp9x-low ES cells. **a)** ChIP recovery before sequencing recapitulates the global gain of H3K27me3 in Usp9x-high ES cells (Fig. 3a). **b)** Spike in-normalized sequencing coverage of H3K27me3 in the indicated cells. **c)** H3K27me3 coverage in Usp9x-high or Usp9x-low cells over bivalent peaks, a random peak set of the same size (2566), or all peaks found in ES cells at baseline (no auxin). **d)** Representative genome browser view of H3K27me3 signal in Usp9x-high and Usp9x-low cells. Elevated H3K27me3 signal in Usp9x-high cells is often observed outside of promoters. Data are mean \pm s.d. of 2 replicates (a) or sum of replicates (b-d). Boxplot hinges (c) show the first and third quartiles, with median center line. **** $P < 0.0001$ by Wilcoxon rank-sum test (c).



1043
 1044
 1045
 1046
 1047
 1048
 1049
 1050
 1051

Supplementary Figure 5. Validation of the Usp9x-PRC2 regulatory interaction. **a)** Co-IP showing that GFP-tagged Usp9x interacts with Suz12 and Ezh2 in AID-Usp9x cells. **b)** Acute catalytic inhibition of Usp9x with the semi-selective inhibitor WP1130 leads to gain of ubiquitin at PRC2 proteins, similar to Fig. 4c. WP1130 treatment ranges from 0-4h. **c)** Comparison of wt versus catalytic-dead Usp9x catalytic domain overexpression but in wild-type ES cells, similar to Fig. 4d. Asterisk (*) designates the expected band size for the Usp9x catalytic domain construct. All western blots are representative of 2-3 biological replicates.

1052 **SUPPLEMENTARY REFERENCES**

- 1053 97. Ran, F. A. *et al.* Genome engineering using the CRISPR-Cas9 system. *Nat Protoc* **8**, 2281–
1054 2308 (2013).
- 1055 98. Seiler, C. Y. *et al.* DNASU plasmid and PSI:Biological-Materials repositories: resources to
1056 accelerate biological research. *Nucleic Acids Res* **42**, D1253–D1260 (2014).
- 1057 99. Liu, H. & Naismith, J. H. An efficient one-step site-directed deletion, insertion, single and
1058 multiple-site plasmid mutagenesis protocol. *BMC biotechnology* **8**, 91 (2008).
- 1059 100. Kim, D. *et al.* TopHat2: accurate alignment of transcriptomes in the presence of insertions,
1060 deletions and gene fusions. *Genome Biol* **14**, R36 (2013).
- 1061 101. Law, C. W., Chen, Y., Shi, W. & Smyth, G. K. voom: Precision weights unlock linear model
1062 analysis tools for RNA-seq read counts. *Genome Biol* **15**, R29 (2014).
- 1063 102. Love, M. I., Huber, W. & Anders, S. Moderated estimation of fold change and dispersion for
1064 RNA-seq data with DESeq2. *Genome Biol* **15**, 550 (2014).
- 1065 103. Ashburner, M. *et al.* Gene Ontology: tool for the unification of biology. *Nat Genet* **25**, 25–29
1066 (2000).
- 1067 104. Huang, D. W., Sherman, B. T. & Lempicki, R. A. Bioinformatics enrichment tools: paths
1068 toward the comprehensive functional analysis of large gene lists. *Nucleic Acids Res* **37**, 1–13
1069 (2009).
- 1070 105. Mi, H., Muruganujan, A., Ebert, D., Huang, X. & Thomas, P. D. PANTHER version 14:
1071 more genomes, a new PANTHER GO-slim and improvements in enrichment analysis tools.
1072 *Nucleic Acids Res* **47**, D419–D426 (2019).
- 1073 106. Carbon, S. *et al.* The Gene Ontology Resource: 20 years and still GOing strong. *Nucleic*
1074 *Acids Res* **47**, D330–D338 (2018).
- 1075 107. Chen, E. Y. *et al.* Enrichr: interactive and collaborative HTML5 gene list enrichment
1076 analysis tool. *Bmc Bioinformatics* **14**, 128 (2013).
- 1077 108. Macfarlan, T. S. *et al.* Embryonic stem cell potency fluctuates with endogenous retrovirus
1078 activity. *Nature* **487**, 57–63 (2012).
- 1079 109. Wamstad, J. A. *et al.* Dynamic and coordinated epigenetic regulation of developmental
1080 transitions in the cardiac lineage. *Cell* **151**, 206–220 (2012).
- 1081 110. Gu, G. *et al.* Global expression analysis of gene regulatory pathways during endocrine
1082 pancreatic development. *Development* **131**, 165–179 (2004).
- 1083 111. Barry, C. *et al.* Uniform neural tissue models produced on synthetic hydrogels using
1084 standard culture techniques. *Exp Biol Med* **242**, 1679–1689 (2017).

- 1085 112. Shechter, D., Dormann, H. L., Allis, C. D. & Hake, S. B. Extraction, purification and
1086 analysis of histones. *Nat Protoc* **2**, 1445–1457 (2007).
- 1087 113. Mendez, J. & Stillman, B. Chromatin association of human origin recognition complex,
1088 cdc6, and minichromosome maintenance proteins during the cell cycle: assembly of
1089 prereplication complexes in late mitosis. *Molecular and Cellular Biology* **20**, 8602–8612 (2000).
- 1090 114. Langmead, B. & Salzberg, S. L. Fast gapped-read alignment with Bowtie 2. *Nature*
1091 *Methods* **9**, 357–359 (2012).
- 1092 115. Ramírez, F. *et al.* deepTools2: a next generation web server for deep-sequencing data
1093 analysis. *Nucleic Acids Res* **44**, W160-5 (2016).
- 1094 116. Leek, J. T., Johnson, W. E., Parker, H. S., Jaffe, A. E. & Storey, J. D. The sva package for
1095 removing batch effects and other unwanted variation in high-throughput experiments.
1096 *Bioinformatics* **28**, 882–883 (2012).
- 1097 117. Gao, Y. *et al.* Protein Expression Landscape of Mouse Embryos during Pre-implantation
1098 Development. *Cell Reports* **21**, 3957–3969 (2017).
- 1099 118. Israel, S. *et al.* An integrated genome-wide multi-omics analysis of gene expression
1100 dynamics in the preimplantation mouse embryo. *Sci Rep-uk* **9**, 13356 (2019).
- 1101 119. DiTroia, S. P. *et al.* Maternal vitamin C regulates reprogramming of DNA methylation and
1102 germline development. *Nature* **573**, 271–275 (2019).